Autonomous Robots manuscript No.
(will be inserted by the editor)

Complete 3-D Dynamic Coverage in Energy-constrained Multi-UAV Sensor Networks

William Bentz · Tru Hoang · Enkhmurun Bayasgalan · Dimitra Panagou

Received: date / Accepted: date

Abstract This paper considers dynamic coverage control of multiple power-constrained agents subject to 3D rigid body kinematics. The agents are deployed to patrol a domain until the entire space has reached a satisfactory level of coverage. This is achieved through the gathering of information by a forward-facing sensor footprint, modelled as an anisotropic spherical sector. Coverage and collision avoidance guarantees are met by a hybrid controller consisting of four operating modes: local coverage, global coverage, waypoint scan and subdomain transfer. Energy-aware methods are encoded into the global coverage state to shift the bulk of spatial redistribution onto less constrained agents. Additionally, a novel domain partitioning strategy is used that directs individual agents to explore within concentric hemispherical shells around a centralized charging station. This results in flight paths that are guaranteed to terminate at the charging station in the limit that agent batteries expire. The efficacy of this algorithm is presented through experimental trials with three agents in an indoor environment. Simulations are provided for ten agents.

Keywords Coverage · Multi-robot cooperation · Aerial robots · Autonomous vehicle

1 Introduction

The past decade has seen rapid improvements in the performance of small unmanned aircraft systems (sUAS) and a continued miniaturization of low-cost sensors. Combined, these mobile wireless sensor networks (MWSNs) are useful in a wide range of military and civilian applications including: battlefield and traffic surveillance, search and rescue operations, and environmental monitoring (Abazeed et al 2013; Zhang et al 2013). In the latter application, scientists studying global warming require 3-D gas concentration maps surrounding carbon dioxide and methane sources and sinks. Current efforts, such as the NASA Atmospheric Infrared Sounder, utilize satellite-based observations to build concentration maps. Though satellites offer large horizontal coverage, their vertical resolutions are insufficient for many climate based studies, such as tropopause folding, and may be greatly supplemented by sUAS in situ data (Berman et al 2012; Chahine et al 2008).

Perhaps the greatest operational limitation of sUAS based MWSNs is their reliance upon Lithium Polymer batteries which are typically exhausted in 10-20 minutes. Any real-world implementation will require the frequent return of vehicles to a ground charging station. This work presents a 3D dynamic coverage protocol tailored to this operational requirement.

The authors would like to acknowledge the support of the Automotive Research Center (ARC) in accordance with Cooperative Agreement W56HZV-14-2-0001 U.S. Army TARDEC in Warren, MI and the support by an Early Career Faculty grant from NASAs Space Technology Research Grants Program.

W. Bentz (✉) · T. Hoang · E. Bayasgalan · D. Panagou
Department of Aerospace Engineering, University of Michigan, 1320 Beal Ave, Ann Arbor, MI
E-mail: wbentz@umich.edu Tel.: +1-717-635-5172

T. Hoang
E-mail: truhoang@umich.edu

E. Bayasgalan
E-mail: murunb@umich.edu

D. Panagou
E-mail: dpanagou@umich.edu

Numerous authors have addressed 2D static coverage problems (Cortes et al 2004; Kwok and Martínez 2008). These are often referred to as area coverage, k-coverage, or point coverage and the solutions typically concern directing the agents towards the centroids of Voronoi tesselations (Zhu et al 2012; Liang et al 2014). A common theme is that each agent seeks to converge upon a fixed position in space to yield satisfactory steady-state coverage.

Dynamic coverage problems traditionally involve limited sensing range mobile agents patrolling a domain in order to cover all points up to a satisfactory level over time. This is essentially a patrol protocol. The 2D case of this problem has been treated extensively in Stipanović et al (2013), Hussein and Stipanović (2007), and Liu et al (2013) with the addition of information decay in Hübel et al (2008). The similar 2D persistent coverage problem includes the periodic servicing requirement of discrete points (Hokayem et al 2007; Song et al 2013; Franco et al 2015).

Static coverage of 3D environments is presented in Oktug et al (2008). The authors extend the classic problems of node scheduling and area coverage to a rough terrain modelled after Encanto Park, Phoenix. Furthermore, they present a novel airdrop-based deployment strategy designed around potential aircraft flight paths. Sensor locations remain fixed in space in Piciarelli et al (2011), and Xie and Zhang (2013). The authors of Piciarelli et al (2011) derive the optimal configurations of Pan-Tilt-Zoom cameras to maximize coverage, while the authors of Xie and Zhang (2013) utilize isotropic conical sensing models. In Cheng et al (2008), the authors explore dynamic coverage control in quasi-3D domains as the agents are tasked to cover the surfaces of non-planar 3D objects.

The most common coverage formulation associated with UAVs in the literature has been sweep coverage. The authors of Smith et al (2012) consider preplanned paths for two aerial robots which continuously sweep downward facing sensors over a field. Coverage decays linearly in time for portions of the field which lie outside of the sensing footprints. Collision avoidance is implicit by using a separate fixed flight altitude for each agent. The authors of Nam et al (2016) also consider offline trajectory generation for fixed altitude flights but provide outdoor experimental results with a single Ascending Technologies Pelican. In Arajo et al (2013), the authors use domain partitioning to construct parallel lanes in which UAV's may cover simultaneously. However, only a fixed-wing single agent is demonstrated experimentally.

In Cole et al (2009) and Tisdale et al (2009), the authors conducted technically rigorous outdoors experiments with multiple fixed-wing UAV's attempting to localize ground based targets using vision-based sensors. However, once again the flights paths were restricted to fixed altitudes in order to guarantee collision avoidance.

The authors of Leahy et al (2016) present experiments validating an energy-aware surveillance protocol for multiple quadrotors. Trajectories are generated by dividing the domain into a grid of cubes, each of which contains a vector field. The field may flow entirely inward to a cube thus directing the agent to hover or it may flow outward through one surface to direct the agent to an adjacent cube. This work only allows for one quadrotor to fly at a time and the agents are provided three separate charging stations. This work does not model the sensing capability of the agents and surveillance is described in terms of persistently routing the agents between a small set of regions of interest.

In Yang et al (2013) and Mitchell et al (2015), the authors consider sweep coverage with agents of homogeneous and fixed battery lifespans. To continue covering, the agents must periodically direct themselves to charging stations. These works are graph theoretic in nature and consider discrete points of interest in a 2-D plane. Neither paper presents a realistic model for agent kinematics or control. Yang et al (2013) considers a centralized charging station and attempts to determine the minimum number of agents and their associate paths that will allow for a sufficient number of battery swaps while providing adequate service. Mitchell et al (2015) considers a set of distributed charging stations and provides analysis on the suboptimal Hamiltonian paths between target points. Our work differentiates itself from Yang et al (2013) and Mitchell et al (2015) in that it considers heterogeneous battery lifespans. Furthermore, our agents are subject to 3-D rigid body kinematics and must fully cover the entire volume of the domain.

To the best of our knowledge, no previous work has presented an energy-aware deployment and guidance protocol for a multi-agent 3D dynamic coverage network that accounts for persistent battery replacements. This paper builds upon the authors' previous local and global coverage control strategies developed throughout Panagou et al (2016, in press), Bentz and Panagou (2016), and Bentz and Panagou (2017) which drive the exploration of domains such that each point is covered up to a satisfactory level over time. The novel contributions of this paper will be the derivation of an energy-aware hybrid control strategy that dynamically repartitions the domain such that trajectories are guaranteed to converge upon a single charging station in the limit that each agent's battery expires. Furthermore, this work presents an upper bound on the number of

agents that may be serviced by a single charging station.

This paper is organized as follows: Sect. 2 presents the kinematic and sensing models, as well as an overview of the hybrid control strategy. The control strategies applicable in each of the hybrid modes are presented in Sect. 3. A series of experiments and simulations are presented in Sect. 4. Sect. 5 contains final concluding remarks and outlines future work. Sect. 6 is an appendix of further supporting evidence.

2 Problem formulation

2.1 System model

In this work, we derive a set of kinematic guidance laws which shall be issued to a standard low-level proprietary controller on-board our off-the-shelf quadrotor team. The inputs to this controller are the three body-fixed Cartesian linear velocities and a body-fixed z-axis angular velocity.

We assume our network of mobile agents indexed $i \in \{1, ..., N\}$ is subject to 3-D rigid body kinematics (Beard 2008):

$$\begin{bmatrix} \dot{x}_i \\ \dot{y}_i \\ \dot{z}_i \end{bmatrix} = \begin{bmatrix} \cos\Theta_i \cos\Psi_i & \sin\Phi_i \sin\Theta_i \cos\Psi_i - \cos\Phi_i \sin\Psi_i & \cos\Phi_i \sin\Theta_i \cos\Psi_i + \sin\Phi_i \sin\Psi_i \\ \cos\Theta_i \sin\Psi_i & \sin\Phi_i \sin\Theta_i \sin\Psi_i + \cos\Phi_i \cos\Psi_i & \cos\Phi_i \sin\Theta_i \sin\Psi_i - \sin\Phi_i \cos\Psi_i \\ -\sin\Theta_i & \sin\Phi_i \cos\Theta_i & \cos\Phi_i \cos\Theta_i \end{bmatrix} \begin{bmatrix} u_i \\ v_i \\ w_i \end{bmatrix}, \quad (1)$$

$$\begin{bmatrix} \dot{\Phi}_i \\ \dot{\Theta}_i \\ \dot{\Psi}_i \end{bmatrix} = \begin{bmatrix} 1 & \sin\Phi_i \tan\Theta_i & \cos\Phi_i \tan\Theta_i \\ 0 & \cos\Phi_i & -\sin\Phi_i \\ 0 & \sin\Phi_i \sec\Theta_i & \cos\Phi_i \sec\Theta_i \end{bmatrix} \begin{bmatrix} q_i \\ r_i \\ s_i \end{bmatrix}, \quad (2)$$

where $p_i = [x_i \;\; y_i \;\; z_i]^T$ is the position vector and $\Omega_i = [\Phi_i \;\; \Theta_i \;\; \Psi_i]^T$ is the vector of 3-2-1 Euler angles taken with respect to a global Cartesian coordinate frame $\mathcal{G}$ with origin $\mathcal{O}$. The linear velocities $[u_i \;\; v_i \;\; w_i]^T$ and angular velocities $[q_i \;\; r_i \;\; s_i]^T$ are both expressed in the body fixed frame $\mathcal{B}_i$ with origin p_i. The state vector of agent i is defined as $\tilde{q}_i = [p_i^T \;\; \Omega_i^T]^T$ and the control inputs are u_i, v_i, w_i and s_i respectively. The rotation matrices in (1) and (2) shall be denoted $\mathcal{R}_1$ and $\mathcal{R}_2$ respectively for the remainder of the paper. The agents are confined to stationary hemispherical domain, $\mathcal{D} \subset \mathbb{R}^3$ of radius $\bar{R}_{\mathcal{D}}$, which must be fully surveyed.

Each agent i is equipped with a forward-facing sensor, whose footprint shall be referred to as $\mathcal{S}_i$. A spherical sector model is chosen for $\mathcal{S}_i$ which builds upon our previous work in Panagou et al (2016, in press) and Bentz and Panagou (2016) by rotating the 2-D sensing footprint 180° about its center line. The sensing data provided by $\mathcal{S}_i$ is anisotropic in nature; that is, it degrades in quality towards the periphery of the footprint. This is encoded through the definition of the sensing constraint functions for each agent i:

$$c_{1i} = \beta_i R_i^2 - (\tilde{x} - x_i)^2 - (\tilde{y} - y_i)^2 - (\tilde{z} - z_i)^2, \quad (3a)$$

$$c_{2i} = \alpha_i - \phi_i, \quad (3b)$$

for $\beta_i = \min\{1, \mu_i \left((\tilde{x} - x_i)^2 + (\tilde{y} - y_i)^2 - (\tilde{z} - z_i)^2\right)\}$ with real constant $\mu_i >> 1$. R_i is the sensing range, $\tilde{p}_i = [\tilde{x} \;\; \tilde{y} \;\; \tilde{z}]^T$ is the position of a point within $\mathcal{S}_i$ with respect to $\mathcal{G}$, α_i is the angle between the periphery and centerline of the spherical sector (the $\hat{x}_{\mathcal{B}_i}$ axis), and ϕ_i is the angle between $r_{\tilde{p}_i/p_i} = \tilde{p}_i - p_i$ (resolved in $\mathcal{G}$ by construction) and the $\hat{x}_{\mathcal{B}_i}$ axis given as the inverse cosine of the dot product of $\hat{r}_{\tilde{p}_i/p_i}$ and $\hat{x}_{\mathcal{B}_i}$ resolved in $\mathcal{G}$:

$$\phi_i = \arccos\left(\hat{r}_{\tilde{p}_i/p_i} \cdot \hat{x}_{\mathcal{B}_i}|_{\mathcal{G}}\right). \quad (4)$$

Note that:

$$\hat{r}_{\tilde{p}_i/p_i} = \frac{1}{\sqrt{(\tilde{x} - x_i)^2 + (\tilde{y} - y_i)^2 + (\tilde{z} - z_i)^2}} \begin{bmatrix} (\tilde{x} - x_i) \\ (\tilde{y} - y_i) \\ (\tilde{z} - z_i) \end{bmatrix},$$

and $\hat{x}_{\mathcal{B}_i}|_{\mathcal{G}}$ is determined by multiplying $\mathcal{R}_1$ by $[1 \;\; 0 \;\; 0]^T$:

$$\hat{x}_{\mathcal{B}_i}|_{\mathcal{G}} = \begin{bmatrix} \cos\Psi_i \cos\Theta_i \\ \sin\Psi_i \cos\Theta_i \\ -\sin\Theta_i \end{bmatrix}.$$

Agent i is thus capable of detecting objects that lie within an angle of $2\alpha_i > 0$ about the $\hat{x}_{\mathcal{B}_i}$ axis and a range of $R_i > 0$. Assume that the body of agent i may be bounded with a sphere of radius $\mathscr{r}_i$ centered at p_i. This model for agent i is depicted in Fig. 1. Let

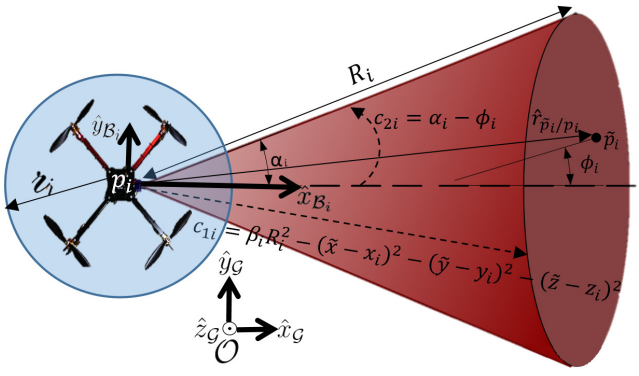

Fig. 1 The body of agent i is bounded by a sphere of radius $\mathscr{r}_i$ and possesses $\mathcal{S}_i$.

us denote $\max\{0, c_{ki}\} = C_{ki}$. One can define the sensing function that represents the quality of information

available at each point over the sensing domain as:

$$S_i(\tilde{q}_i,\tilde{p}) = \begin{cases} \frac{C_{1i}C_{2i}}{C_{1i}+C_{2i}}, & \text{if } card\left(\bar{C}_i\right) < 2 \wedge r_{\tilde{p}_i/p_i} > 0; \\ 0, & \text{otherwise,} \end{cases} \tag{5}$$

where $\bar{C}_i$ is the set of zero elements in C_{ki}. $S_i(\tilde{q}_i,\tilde{p})$ takes a value of zero outside of $\mathcal{S}_i$. Note that $S_i(\tilde{q}_i,\tilde{p})$ is defined over all of $\mathcal{D}$ and thus has static bounds. $S_i(\tilde{q}_i,\tilde{p})$ is continuous in $\tilde{p}$ while taking a value of zero along $\partial\mathcal{S}_i$. In verifying this continuity, it is important to note that $S_i(\tilde{q}_i,\tilde{p})$ approaches zero from within $\mathcal{S}_i$ in the limit that either $card\left(\bar{C}_i\right) = 2$ or $r_{\tilde{p}_i/p_i} = 0$ are satisfied. The former condition may be verified by taking a limit of the first piecewise definition of (5) as C_{1i} and C_{2i} tend to zero. The latter condition results from our definition of β_i.

Define the coverage level provided by agent i at time t as:

$$Q_i(t,\tilde{p}) = \int_0^t S_i\left(\tilde{q}_i(\tau),\tilde{p}\right)\, d\tau. \tag{6}$$

This summed over each agent produces the global coverage level:

$$Q(t,\tilde{p}) = \sum_{i=1}^{N} Q_i(t,\tilde{p}). \tag{7}$$

Remark 1 In this work, coverage refers to the accumulation of sensing data over time. The effect of agent i's motion is to vary the points $\tilde{p} \in \mathcal{D}$ for which $S_i(\tilde{q}_i,\tilde{p})$ is nonzero. The domain $\mathcal{D}$ is said to be fully covered at a final time t_f when $Q(t_f,\tilde{p}) \geq C^\star, \forall \tilde{p} \in \mathcal{D}$ where $C^\star$ is a predefined desired coverage level. Full coverage is equivalent to driving the global coverage error, defined in Sect. 3.1.1, to zero.

Assumption 1 A communication network is employed such that agent i has access to $Q(t,\tilde{p})$ as well as $q_j(t)$ and $V_j(t), \forall j \in \{1,...,N\}$ where $V_j(t)$ is the battery voltage of agent j.

2.2 Network safety through energy-aware deployment

While previous works, such as Atinc et al (2014) and Hussein and Stipanović (2007), have considered network safety in terms of collision avoidance, few have incorporated realistic power limitations. The mobile sensing agents considered in this work are typical in that they rely upon a constrained on-board power source (e.g., a battery) which must be periodically replaced at a centralized station. Failure to do so will result in agents becoming stranded and potentially compromised. Consider that each agent $i \in \{1,...,N\}$ is powered by a battery with voltage $V_i(t)$, whose initial value at deployment time t_i^d is $V_i(t_i^d) = V_0$. Define the cutoff voltage, V^{co} as the minimum voltage for which an agent may fly reliably. V^{co} shall satisfy $V_i(t_i^{co}) = V^{co}$, where t_i^{co} is the cutoff time. Define agent i's nominal battery lifespan T_i to satisfy $T_i = t_i^{co} - t_i^d$. If agent i is deployed at time t_i^d and lands at time t_i^{co}, then it shall hold for a waiting period T_i^w before redeployment. T_i^w shall satisfy $T_i + T_i^w = T^\star$ where $T^\star$ is an upper bound on the maximum battery lifespan of any agent in the network.

Assumption 2 If at time t_i^{co}, p_i converges upon $\mathcal{O}$, then the voltage of agent i shall be restored such that $V_i(t_i^{co} + T_i^w) = V_0$.

This assumption is used to model the scenario in which a ground servicing station is present at the origin. The agents are required to land periodically at a centralized station to have their batteries switched out for fully charged ones. This scenario is presented in Fig. 2.

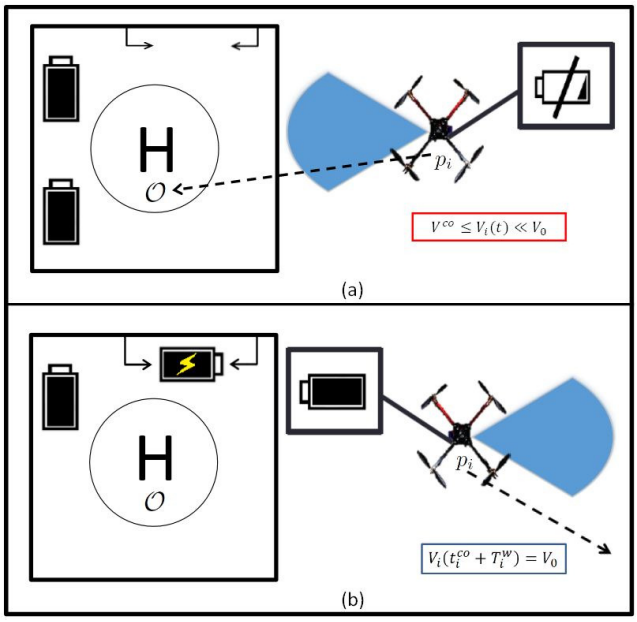

Fig. 2 Agent i lands upon a helipad at $\mathcal{O}$ as $V_i(t) \to V^{co}$. After a waiting period, T_i^w, the voltage is instantaneously restored to V_0.

Definition 1 Two agents i and j are said to be collision-free so long as $\|p_i(t) - p_j(t)\| > \text{ż}_i + \text{ż}_j$, $\forall t$.

Remark 2 Safety is guaranteed $\forall\, i$ as long as 1) $V_i(t) \geq V^{co}$, $\forall t$ and $V_i = V^{co} \implies p_i = \mathcal{O}$ and 2) i avoids collisions with all agents $j \neq i$.

The purpose of this work is to develop and demonstrate techniques that will achieve the goals of *Remark 1* and *Remark 2*. This will require the use of four unique modes of operation, termed local coverage mode, global coverage mode, subdomain transfer mode, and waypoint scan mode which shall be elaborated upon in the following section. These four modes may be represented by five hybrid states.

2.3 Overview

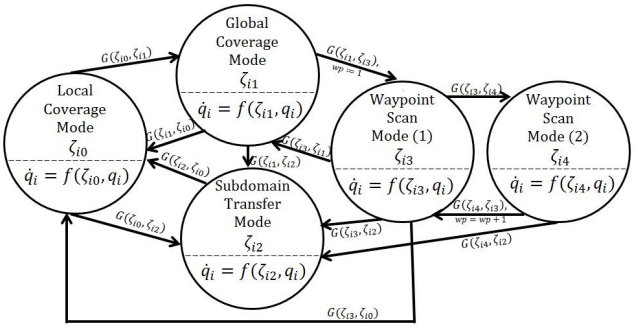

Fig. 3 Agent i operates in accordance with this automaton.

The coverage strategy for agent i may be represented by the hybrid automaton in Fig. 3. Note that each agent operates in accordance with its own automaton and thus an arbitrary number of agents may be in any operating mode at any given time. Before proceeding, it is prudent to provide a brief overview of the purpose of each mode.

Local coverage refers to the active exploration of $\mathcal{D}$ by agent i. In this mode, the agent continuously seeks to orient and translate $\mathcal{S}_i$, such that the portion of uncovered space within $\mathcal{S}_i$ is increased. This is conceptually similar to following the gradient of the coverage error. This mode becomes ineffective if and when the immediate volume of space surrounding the agent has been fully covered and no infinitesimal translation or rotation of $\mathcal{S}_i$ will increase the volume of uncovered space within $\mathcal{S}_i$. Thus, when the rate of change of the global coverage error by agent i drops below some threshold, global coverage mode is activated.

Global coverage selects a waypoint for agent i to travel to before resuming local coverage. If the aforementioned threshold is still violated at the waypoint, the agent will switch into waypoint scan mode in order to perform one final sweep of the waypoint's local area. Waypoint scan mode (1) guides agents between a set of 13 sub-waypoints which surround the immediate vicinity of the global coverage waypoint. Waypoint scan mode (2) controls a 360° yaw revolution of $\mathcal{S}_i$ at each sub-waypoint. Upon completion of this scan the agent typically uses global coverage to select a new waypoint at which it may attempt to resume local coverage.

The final operating mode, subdomain transfer, is used to transfer agents between subdomain partitions of $\mathcal{D}$. These subdomains are concentric hemispherical shells which surround a battery charging station. As an agent's battery expires, it is continually transfered to interior subdomains until it occupies the innermost shell whose boundaries converge upon the charging station in the limit that the battery expires. Subdomain transfer is activated from any other mode if the agent exceeds some distance from the charging station.

A rigorous definition of all entities of the automaton, including the guard conditions present in Fig. 3, is presented in Appendix 6.1.

3 Control strategy

3.1 Local coverage mode

3.1.1 Nominal control strategy

Local coverage is the nominal mode that directs active exploration by the agents. Define the global coverage error with respect to $C^\star$ as:

$$E(t) = \int_{\mathcal{D}} h(C^\star - Q(t, \tilde{p}))\, d\tilde{p}. \tag{8}$$

where $h(w) = (\max\{0, w\})^3$ with first derivative $h' = \frac{dh}{dw} = 3(\max\{0, w\})^2$ and second derivative $h'' = \frac{d^2h}{dw^2} = 6(\max\{0, w\})$. The nominal control strategy will be derived via differentiation of (8), a volume integral, so a few mathematical preliminaries are required.

Recall the generalized transport theorem (Slattery 1999):

$$\frac{d}{dt}\int_{R_{(s)}} f dV = \int_{R_{(s)}} \frac{\partial f}{\partial t}\, dV + \int_{S_{(s)}} f \mathbf{v}_{(\mathbf{s})} \cdot \mathbf{n}\, dA \tag{9}$$

where f is any scalar-, vector-, or tensor-valued function of position and time, $S_{(s)}$ is the boundary of the volume $R_{(s)}$ over which f is integrated, $\mathbf{n}$ is the unit vector normal to the boundary, and $\mathbf{v}_{(\mathbf{s})}$ is the velocity of the boundary. V and A refer to volume and area respectively. Invoking (9) allows for differentiation of (8) with respect to time:

$$\begin{aligned}\dot{E}(t) = &\int_{\mathcal{D}} h'(C^\star - Q(t, \tilde{p}))\left(\frac{-\partial Q(t, \tilde{p})}{\partial t}\right) d\tilde{p} \\ &+ \int_{\partial\mathcal{D}} \big(h(C^\star - Q(t, \tilde{p}))\big)\mathbf{v}_{(\mathbf{s})} \cdot \mathbf{n}\, dA,\end{aligned} \tag{10}$$

where $\partial\mathcal{D}$ is the boundary of $\mathcal{D}$. The control volume is $\mathcal{D}$ which is time invariant and thus $\mathbf{v}_{(\mathbf{s})} = 0$. Further justification for differentiation under the integral sign of (8) is presented in Appendix 6.2. This expression reduces to:

$$\dot{E}(t) = \int_D h'(C^\star - Q(t,\tilde{p}))\left(\frac{-\partial Q(t,\tilde{p})}{\partial t}\right) d\tilde{p}, \tag{11}$$

which expands to:

$$\begin{aligned}\dot{E}(t) &= -\int_D h'(C^\star - Q(t,\tilde{p}))\sum_{i=1}^{N} S_i(\tilde{q}_i(t),\tilde{p})d\tilde{p} \\ &= -\sum_{i=1}^{N}\int_D h'(C^\star - Q(t,\tilde{p}))S_i(\tilde{q}_i(t),\tilde{p})d\tilde{p} \\ &= \sum_{i=1}^{N}\hat{e}_i(t),\end{aligned} \tag{12}$$

where the definition of $\hat{e}_i(t)$ is implicit. (12) is less than or equal to zero. Therefore, (8) is non-increasing. In fact, $\dot{E}$ may only take zero value at some time $t^\star$ if $\forall i \in N,\ Q(t^\star,\tilde{p}) \geq C^\star\ \forall \tilde{p} \in D \mid S_i(\tilde{q}_i(t^\star),\tilde{p}) > 0$. Moving forward, the strategy will be to design control laws that drive (12) to be increasingly negative.

Taking the derivative of (12) with respect to time yields:

$$\ddot{E}(t) = \sum_{i=1}^{N}\dot{\hat{e}}_i(t) \tag{13}$$

following once again from (9). $\dot{\hat{e}}_i(t)$ is defined as:

$$\begin{aligned}\dot{\hat{e}}_i(t) = -\int_{D_i} &(-h''(C^\star - Q(t,\tilde{p}))S_i(\tilde{q}_i(t),\tilde{p})(S_i(\tilde{q}_i(t),\tilde{p}) \\ &+h'(C^\star - Q(t,\tilde{p}))\frac{d}{dt}(S_i(\tilde{q}_i(t),\tilde{p}))\Big) d\tilde{p}.\end{aligned} \tag{14}$$

The sensing footprint is independent of Φ_i assuming that the centerline of the spherical sector is aligned with the $\hat{x}_{\mathcal{B}_i}$ axis. $\frac{d}{dt}(S_i(\tilde{q}_i(t),\tilde{p}))$ is expanded in (15) and through the definitions in (16-21) one may restate (14) as (22).

If one were to command zero inputs to this system, it becomes clear that (16) may be physically interpreted as the rate at which the coverage rate is reducing due to information saturation at any particular position and orientation of the sensing footprint, $\mathcal{S}_i$. As the footprint remains stationary, there are diminishing returns on the value of newly acquired information. Thus, the additional terms in (22) allow for the coverage rate to be increased by mobilizing the sensor. One strategy is to define the following control law:

$$u_i{}^{loc} = k_u^{loc}\ a_{i1}(t, Q(t,\tilde{p})), \tag{23a}$$
$$v_i{}^{loc} = k_v^{loc}\ a_{i2}(t, Q(t,\tilde{p})), \tag{23b}$$
$$w_i{}^{loc} = k_w^{loc}\ a_{i3}(t, Q(t,\tilde{p})), \tag{23c}$$
$$s_i{}^{loc} = k_s^{loc}\ a_{i5}(t, Q(t,\tilde{p})), \tag{23d}$$

which drives (22) to smaller and ideally negative values with the intent of preventing (12) from reaching zero. (23a-d) tends to drive i to increase the portion of uncovered space intersecting $\mathcal{S}_i$ at any given time. This strategy alone cannot guarantee that the global coverage error, $E(t)$, will converge to zero. Rather, this guarantee is met with the introduction of additional hybrid modes and proven in Sect. 3.5. Note that superscripts associated with control inputs denote the applicable operating mode: e.g., *loc* for local coverage, *glo* for global coverage etc.

3.1.2 Collision avoidance augmentation

Collision avoidance, as defined in *Definition 1*, may be encoded directly into the local coverage control strategy (23) through a straightforward modification to the global coverage level (7)–a technique the authors refer to as map augmentation. Further map augmentation of (7) will be presented in Sect. 3.1.3 to produce additional desired effects.

Consider agent i which must avoid agent j. Define the buffer distance of i from j as $R_{b,ij} = R_i + r_i + r_j$. Define the coverage map avoidance term:

$$\acute{Q}_{ij}(t,\tilde{p}) = \begin{cases} C^\star, & \text{if } \tilde{p} \in \bar{B}_{R_{b,ij}}(p_j); \\ 0, & \text{otherwise,}\end{cases} \tag{24}$$

and $\bar{B}_{R_{b,ij}}(p_j)$ is the closed ball of radius $R_{b,ij}$ centered at p_j. $\acute{Q}_{ij}(t,\tilde{p})$ may augment the global coverage map for i as follows:

$$\acute{Q}_i(t,\tilde{p}) = Q(t,\tilde{p}) + \sum_{j=1}^{N-1}\acute{Q}_{ij}(t,\tilde{p}). \tag{25}$$

$\acute{Q}_i(t,\tilde{p})$ is the avoidance augmented global coverage map for agent i. This term allows agent i to perceive a closed ball of space around j as fully covered if the agents come into close proximity. This effect is realized by substituting $\acute{Q}_i(t,\tilde{p})$ for $Q(t,\tilde{p})$ in the proposed local coverage control law (23):

$$\acute{u}_i{}^{loc} = k_u^{loc}\ a_{i1}(t, \acute{Q}_i(t,\tilde{p})), \tag{26a}$$
$$\acute{v}_i{}^{loc} = k_v^{loc}\ a_{i2}(t, \acute{Q}_i(t,\tilde{p})), \tag{26b}$$
$$\acute{w}_i{}^{loc} = k_w^{loc}\ a_{i3}(t, \acute{Q}_i(t,\tilde{p})), \tag{26c}$$
$$\acute{s}_i^{loc} = k_s^{loc}\ a_{i5}(t, \acute{Q}_i(t,\tilde{p})), \tag{26d}$$

Expand $\frac{d}{dt}(S_i(\tilde{q}_i(t),\tilde{p}))$:

$$\begin{aligned}\frac{d}{dt}(S_i(\tilde{q}_i(t),\tilde{p})) &= \frac{\partial S_i}{\partial x_i}\dot{x}_i(t)+\frac{\partial S_i}{\partial y_i}\dot{y}_i(t)+\frac{\partial S_i}{\partial z_i}\dot{z}_i(t)+\frac{\partial S_i}{\partial \Psi_i}\dot{\Psi}_i(t)+\frac{\partial S_i}{\partial \Theta_i}\dot{\Theta}_i(t) = \left(\frac{\partial S_i}{\partial x_i}\cos\Theta\cos\Psi+\frac{\partial S_i}{\partial y_i}\cos\Theta\sin\Psi-\frac{\partial S_i}{\partial z_i}\sin\Theta\right)u_i(t)\\ &+\left(\frac{\partial S_i}{\partial x_i}(\sin\Phi\sin\Theta\cos\Psi-\cos\Phi\sin\Psi)+\frac{\partial S_i}{\partial y_i}(\sin\Phi\sin\Theta\sin\Psi+\cos\Phi\cos\Psi)+\frac{\partial S_i}{\partial z_i}\sin\Phi\cos\Theta\right)v_i(t)\\ &+\left(\frac{\partial S_i}{\partial x_i}(\cos\Phi\sin\Theta\cos\Psi+\sin\Phi\sin\Psi)+\frac{\partial S_i}{\partial y_i}(\cos\Phi\sin\Theta\sin\Psi-\sin\Phi\cos\Psi)+\frac{\partial S_i}{\partial z_i}\cos\Phi\cos\Theta\right)w_i(t)\\ &+\left(\frac{\partial S_i}{\partial \Psi_i}\sin\Phi\sec\Theta+\frac{\partial S_i}{\partial \Theta_i}\cos\Phi\right)r_i(t)+\left(\frac{\partial S_i}{\partial \Psi_i}\cos\Phi\sec\Theta-\frac{\partial S_i}{\partial \Theta_i}\sin\Phi\right)s_i(t).\end{aligned} \tag{15}$$

Now introduce the following definitions:

$$a_{i0}(t,Q(t,\tilde{p})) = \int_{D_i} h''(C^\star - Q(t,\tilde{p}))S_i(\tilde{q}_i(t),\tilde{p})(S_i(\tilde{q}_i(t),\tilde{p})d\tilde{p}, \tag{16}$$

$$a_{i1}(t,Q(t,\tilde{p})) = \int_{D_i} h'(C^\star - Q(t,\tilde{p}))\left(\frac{\partial S_i}{\partial x_i}\cos\Theta\cos\Psi+\frac{\partial S_i}{\partial y_i}\cos\Theta\sin\Psi-\frac{\partial S_i}{\partial z_i}\sin\Theta\right)d\tilde{p}, \tag{17}$$

$$a_{i2}(t,Q(t,\tilde{p})) = \int_{D_i} h'(C^\star - Q(t,\tilde{p}))\left(\frac{\partial S_i}{\partial x_i}(\sin\Phi\sin\Theta\cos\Psi-\cos\Phi\sin\Psi)+\frac{\partial S_i}{\partial y_i}(\sin\Phi\sin\Theta\sin\Psi+\cos\Phi\cos\Psi)+\frac{\partial S_i}{\partial z_i}\sin\Phi\cos\Theta\right)d\tilde{p}, \tag{18}$$

$$a_{i3}(t,Q(t,\tilde{p})) = \int_{D_i} h'(C^\star - Q(t,\tilde{p}))\left(\frac{\partial S_i}{\partial x_i}(\cos\Phi\sin\Theta\cos\Psi+\sin\Phi\sin\Psi)+\frac{\partial S_i}{\partial y_i}(\cos\Phi\sin\Theta\sin\Psi-\sin\Phi\cos\Psi)+\frac{\partial S_i}{\partial z_i}\cos\Phi\cos\Theta\right)d\tilde{p}, \tag{19}$$

$$a_{i4}(t,Q(t,\tilde{p})) = \int_{D_i} h'(C^\star - Q(t,\tilde{p}))\left(\frac{\partial S_i}{\partial \Psi_i}\sin\Phi\sec\Theta+\frac{\partial S_i}{\partial \Theta_i}\cos\Phi\right)d\tilde{p}, \tag{20}$$

$$a_{i5}(t,Q(t,\tilde{p})) = \int_{D_i} h'(C^\star - Q(t,\tilde{p}))\left(\frac{\partial S_i}{\partial \Psi_i}\cos\Phi\sec\Theta-\frac{\partial S_i}{\partial \Theta_i}\sin\Phi\right)d\tilde{p}. \tag{21}$$

One can then rewrite (14) as:

$$\dot{\tilde{e}}_i(t) = a_{i0}(t,Q(t,\tilde{p})) - u_i(t)a_{i1}(t,Q(t,\tilde{p})) - v_i(t)a_{i2}(t,Q(t,\tilde{p})) - w_i(t)a_{i3}(t,Q(t,\tilde{p})) - r_i(t)a_{i4}(t,Q(t,\tilde{p})) - s_i(t)a_{i5}(t,Q(t,\tilde{p})). \tag{22}$$

where $a_{ik}(t,\acute{Q}_i(t,\tilde{p}))$, $\forall k \in \{1,2,3,5\}$, are functions of $\acute{Q}_i(t,\tilde{p})$ rather than $Q(t,\tilde{p})$.

Theorem 1 Assuming both agents are operating under control law (26), agent i may not collide with agent j.

Proof Note that in (17), (18), (19), (20), and (21), each additive term under the integral sign is multiplied by some derivative of $S_i(\tilde{q}_i,\tilde{p})$. Recall from Sect. 2.1 that $S_i(\tilde{q}_i,\tilde{p})$ is identically zero outside of $\mathcal{S}_i$. Therefore, (17), (18), (19), (20), and (21) may be equivalently integrated over $\mathcal{S}_i$ instead of $\mathcal{D}$. This holds true also for the augmented forms in (26). As $\|p_i - p_j\|$ approaches $(\text{ɤ}_i + \text{ɤ}_j)$, $\acute{Q}_i(t,\tilde{p}) \geq C^\star$, $\forall \tilde{p} \in \mathcal{S}_i$. Thus, $\lim_{\|p_i-p_j\|\to(\text{ɤ}_i+\text{ɤ}_j)} a_{ik}(t,\acute{Q}_i(t,\tilde{p})) = 0$, $\forall k \in \{1,2,3,5\}$. Therefore, (26) decay to zero as $\|p_i - p_j\| \to (\text{ɤ}_i + \text{ɤ}_j)$. Agent i comes to rest in this limit (as does agent j which can be demonstrated through the same logic). Agent i and j avoid collision by *Definition 1.* This concludes the proof.

This theoretical guarantee is made with respect to a worst case scenario in which the agents come to rest adjacent to one another. This can only occur if the agents' local space, i.e., $\tilde{p} \in \mathcal{S}_i$, has reached a full coverage level. The two agents would then switch into global coverage mode and make use of the global coverage collision avoidance technique presented in Sect. 3.2. Under nominal circumstances, the natural motion of the agents under (26) would rarely lead to this scenario. Rather, any portion of $\mathcal{S}_i$ which extends outside of $\bar{B}_{R_{b,ij}}(p_j)$ into a portion of $\mathcal{D}$ not fully covered would tend to direct i away from j.

3.1.3 Energy-aware domain partitioning

$\acute{Q}_i(t,\tilde{p})$ may be further augmented to produce a local coverage strategy consistent with the power constrained operational safety requirements of Sect. 2.2. This shall be accomplished through a novel partitioning of the hemisphere $\mathcal{D}$ with radius $\bar{R}_\mathcal{D}$ into concentric hemispherical shell subdomains, $\mathcal{D}_\ell$, $\forall \ell \in \{1,...,N-1\}$, around a centralized hemispherical subdomain, $\mathcal{D}_{i_{cr}}$ of radius $\bar{R}_{cr}$. Each of the N agents shall be assigned to monitor one of the N subdomains. This is illustrated in Fig. 4.

Recall the cutoff voltage, V^{co}, as the minimum voltage for which an agent may fly reliably. In practice,

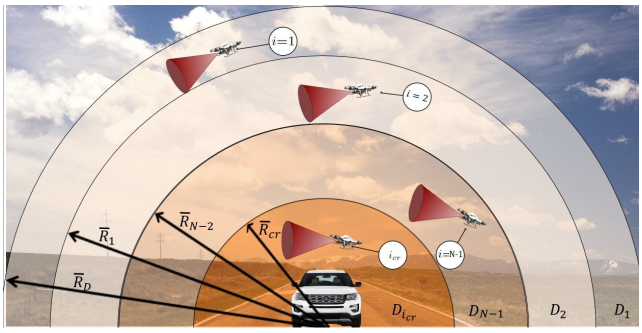

Fig. 4 In the illustrated application, a team of quadrotors patrols the airspace surrounding a ground vehicle charging station. The most power constrained agent, i_{cr} occupies an inner hemisphere $\mathcal{D}_{i_{cr}}$ while the remaining $N-1$ agents occupy subdomains $\mathcal{D}_\ell$, $\forall \ell \in \{1, ..., N-1\}$.

this should be chosen as the minimum voltage that allows for the vehicle to transition from a hovering state through a stable landing sequence. This may be determined experimentally and adjusted depending upon how large of a buffer the user desires.

Of the N agents, define one as the power-critical agent with index i_{cr} where:

$$i_{cr} = \arg\min_i \left(V_i - V^{co}\right). \tag{27}$$

The remaining indices i_ℓ, $\forall \ell \in \{1, ..., N-1\}$ are chosen to satisfy:

$$V_{i_1} > V_{i_2} > ... > V_{i_{N-1}}.$$

Define the power-critical augmented global coverage level for agent i_{cr} as:

$$\acute{Q}_{i_{cr}}(t, \tilde{p}) = \dot{Q}_{i_{cr}}(t, \tilde{p}) + M_{2i_{cr}}(t, \tilde{p}) \tag{28}$$

where:

$$M_{2i_{cr}}(t, \tilde{p}) = \begin{cases} 0, & \text{if } \tilde{p} \in \bar{B}_{\bar{R}_{cr}}(0); \\ C^\star, & \text{otherwise,} \end{cases} \tag{29}$$

and $\bar{R}_{cr}$, as illustrated in Fig. 4, is the operating range of i_{cr} defined as:

$$\bar{R}_{cr} = \min\left(\left(\frac{1}{N}\bar{R}_{\mathcal{D}}^3\right)^{\frac{1}{3}}, \kappa_{i_{cr}}\left(V_{i_{cr}} - V^{co}\right)\right), \tag{30}$$

where $\kappa_{i_{cr}}$ is a tuning parameter. Note that (30) is upper-bounded such that a hemisphere of radius $\bar{R}_{cr}$ would have a maximum possible volume of $\frac{1}{N}$ the volume of $\mathcal{D}$.

The effect above (28) is to encode that agent i_{cr} shall only detect uncovered space within $\mathcal{D}_{i_{cr}}$. As $V_{i_{cr}}$ converges to V^{co}, the domain of interest of i_{cr} converges to the origin. Thus, so long as i_{cr} is capable of entering $\mathcal{D}_{i_{cr}}$ at $t^\star \leq t_{i_{cr}}^{co}$ where $V_{i_{cr}}(t_{i_{cr}}^{co}) = V^{co}$ and remaining within $\mathcal{D}_{i_{cr}}$ until $t_{i_{cr}}^{co}$, then $p_{i_{cr}} \to \mathcal{O}$. The ability to remain within $\mathcal{D}_{i_{cr}}$ shall be guaranteed in *Theorem 2* while the ability to enter $\mathcal{D}_{i_{cr}}$ at or before $t_{i_{cr}}^{co}$ shall be guaranteed through *Theorem 4* in Sect. 3.1.4.

Theorem 2 Assuming that $|\frac{dV_{i_{cr}}(t)}{dt}| \leq |\frac{dV_{i_{cr}}(t)}{dt}|_{t=t_{i_{cr}}^{co}}$, $\forall t \in [t^\star, t_{i_{cr}}^{co}]$, $\kappa_{i_{cr}} < \frac{U_{max}}{|\frac{dV_{i_{cr}}(t)}{dt}|_{t=t_{i_{cr}}^{co}}}$ implies that there exists a control strategy to maintain the condition that $p_{i_{cr}} \in \mathcal{D}_{i_{cr}}$.

Proof Increasing $\kappa_{i_{cr}}$ has the effect of prolonging the time for which i_{cr} spends away from $\mathcal{O}$ which in turn requires a faster terminal rate of convergence in the limit that $V_{i_{cr}}(t) \to V^{co}$. Differentiate $\bar{R}_{cr}$:

$$\dot{\bar{R}}_{cr} = \begin{cases} 0, & \text{if } \kappa_{i_{cr}}\left(V_{i_{cr}} - V^{co}\right) > \left(\frac{1}{N}\bar{R}_D^3\right)^{\frac{1}{3}}; \\ \kappa_{i_{cr}}\frac{dV_{i_{cr}}(t)}{dt}, & \text{otherwise,} \end{cases}, \tag{31}$$

and note that this expression conveys the rate at which $\partial\mathcal{D}_{i_{cr}} \to \mathcal{O}$. In experimental trials it is apparent that the magnitude of $\dot{V}_{i_{cr}}(t)$ tends towards a global maximum in the limit that $V_{i_{cr}}(t) \to V^{co}$. Under this assumption, one may place an upper bound on the magnitude of (31): $|\dot{\bar{R}}_{cr}| \leq \kappa_{i_{cr}}|\frac{dV_{i_{cr}}(t)}{dt}| \leq \kappa_{i_{cr}}|\frac{dV_{i_{cr}}(t)}{dt}|_{t=t_{i_{cr}}^{co}}$ in terms of $\kappa_{i_{cr}}$. Choosing:

$$\kappa_{i_{cr}} < \frac{U_{max}}{|\frac{dV_{i_{cr}}(t)}{dt}|_{t=t_{i_{cr}}^{co}}}, \tag{32}$$

where U_{max} is the maximum linear velocity of the slowest agent in the network, guarantees that $\dot{\bar{R}}_{cr}$, and thus the rate at which $\partial\mathcal{D}_{i_{cr}} \to \mathcal{O}$, will be upper bounded by U_{max}. Thus, assuming that $p_{i_{cr}}(t^\star) \in \mathcal{D}_{i_{cr}}$, there exists a control strategy to guarantee that $p_{i_{cr}}(t) \in \mathcal{D}_{i_{cr}}$, $\forall t \in \left[t^\star, t_{i_{cr}}^{co}\right]$. This concludes the proof.

The goal is to isolate the remaining $N-1$ agents each to their own concentric hemispherical shell subdomain, denoted $\mathcal{D}_\ell$ where $\ell \in \{1, ..., N-1\}$. This guarantees that, at any given time, each $\tilde{p} \in \mathcal{D}$ is within the subdomain of one agent. This is accomplished by assigning $\mathcal{D}_1$ to have outer radius $\bar{R}_{\mathcal{D}}$ and inner radius $\bar{R}_1$, $\mathcal{D}_2$ to have outer radius $\bar{R}_1$ and inner radius $\bar{R}_2$ and similarly up to $\mathcal{D}_{N-1}$ with outer radius $\bar{R}_{N-2}$ and inner radius $\bar{R}_{cr}$.

One logical strategy is to divide the volume of $\mathcal{D} \setminus \mathcal{D}_{i_{cr}}$, that is equal to:

$$V_{rem.} = \frac{1}{2}\left(\frac{4}{3}\pi\left(\bar{R}_{\mathcal{D}}^3 - \bar{R}_{cr}^3\right)\right), \tag{33}$$

equally among each element of $\mathcal{D}_\ell$. This requires $\{\bar{R}_1, \bar{R}_2, ...\bar{R}_{N-2}\}$ to satisfy the following constraint:

$$\begin{aligned}\frac{V_{rem.}}{(N-1)} &= \frac{1}{2}\left(\frac{4}{3}\pi\left(\bar{R}_D^3 - \bar{R}_1^3\right)\right) \\ &= \frac{1}{2}\left(\frac{4}{3}\pi\left(\bar{R}_1^3 - \bar{R}_2^3\right)\right) \\ &\vdots \\ &= \frac{1}{2}\left(\frac{4}{3}\pi\left(\bar{R}_{N-2}^3 - \bar{R}_{cr}^3\right)\right).\end{aligned} \tag{34}$$

This computation is relatively straightforward as a closed form expression exists for $\bar{R}_1$:

$$\bar{R}_1 = \left(\bar{R}_D^3 - \frac{\left(\bar{R}_D^3 - \bar{R}_{cr}^3\right)}{(N-1)}\right)^{\frac{1}{3}} \tag{35}$$

$\{\bar{R}_1, \bar{R}_2, ...\bar{R}_{N-2}\}$ may be found through a sequential chain of computations. The set $\bar{R}_\rho$, $\forall \rho \in \{2, ..., N-2\}$ is defined as:

$$\bar{R}_\rho = \left(\bar{R}_{\rho-1}^3 - \frac{\left(\bar{R}_{\rho-1}^3 - \bar{R}_{cr}^3\right)}{(N-1)}\right)^{\frac{1}{3}}. \tag{36}$$

$\acute{Q}_\ell(t, \tilde{p})$ may be defined similarly to (28). Define:

$$\acute{Q}_\ell(t, \tilde{p}) = \acute{Q}_\ell(t, \tilde{p}) + M_{3\ell}(t, \tilde{p}) \tag{37}$$

where:

$$M_{3\ell}(t, \tilde{p}) = \begin{cases} 0, & \text{if } \tilde{p} \in \mathcal{D}_\ell; \\ C^\star, & \text{otherwise,} \end{cases} \tag{38}$$

and one may substitute $\acute{Q}_\ell(t, \tilde{p})$ for (7) in (12-16) for agents $\ell \in \{1, ..., N-1\}$ and similarly $\acute{Q}_{i_{cr}}(t, \tilde{p})$ for agent i_{cr} to yield the elected local coverage control strategy:

$$\acute{u}_i^{loc} = k_u^{loc}\, a_{i1}(t, \acute{Q}_i(t, \tilde{p})), \tag{39a}$$

$$\acute{v}_i^{loc} = k_v^{loc}\, a_{i2}(t, \acute{Q}_i(t, \tilde{p})), \tag{39b}$$

$$\acute{w}_i^{loc} = k_w^{loc}\, a_{i3}(t, \acute{Q}_i(t, \tilde{p})), \tag{39c}$$

$$\acute{s}_i^{loc} = k_s^{loc}\, a_{i5}(t, \acute{Q}_i(t, \tilde{p})), \tag{39d}$$

3.1.4 An upper bound on N

The ability of agent i_{cr} to enter $\mathcal{D}_{i_{cr}}$ at $t^\star \leq t_{i_{cr}}^{co}$ is dependent upon the number of agents in the network and the scheduling used to temporally space agent deployment. Specifically, there exists an upper bound on N for which agent $i = N-1$ is still within a safe proximity of $\mathcal{O}$ at the instant before selection as i_{cr}. Beyond this bound, the incumbent critical agent cannot transfer to $\mathcal{D}_{i_{cr}}$ before battery expiration. The purpose of this subsection is to define this limit on N and the proper deployment schedule.

Remark 3 With assumed knowledge of the lifespan of each individual agent's battery upon deployment, T_i as defined in Sect 2.2, the network deployment schedule operates such that virtual deployment points occur with a period of $\frac{T^\star}{N}$. The actual deployment of agent i occurs at a time T_i^w greater than the virtual deployment point. With this schedule, it is guaranteed that any agent will have a remaining flight time of $\frac{T^\star}{N}$ at the instant before selection as i_{cr}. This guarantee is provided by *Theorem 3.*

Theorem 3 Assume that $N \geq 2$ agents are deployed one at a time with the deployment schedule and assumptions of *Remark 3.* Then, agent i will have a remaining flight time of $\frac{T^\star}{N}$ at the instant before selection as i_{cr}.

Proof As consistent with the schedule of Remark 3, let us assume that N agents are deployed at the following times:

$$\begin{aligned} t_N^d &= T_N^w \\ t_{N-1}^d &= \frac{T^\star}{N} + T_{N-1}^w \\ t_{N-2}^d &= \frac{2T^\star}{N} + T_{N-2}^w \\ &\vdots \\ t_1^d &= \frac{(N-1)\,T^\star}{N} + T_1^w \end{aligned}$$

From the definition of T_i, we have that $t_i^{co} = t_i^d + T_i$. Thus the cutoff times of the N agents are:

$$\begin{aligned} t_N^{co} &= T_N^w + T_N = T^\star \\ t_{N-1}^{co} &= \frac{T^\star}{N} + T_{N-1}^w + T_{N-1} = \frac{(N+1)\,T^\star}{N} \\ t_{N-2}^{co} &= \frac{2T^\star}{N} + T_{N-2}^w + T_{N-2} = \frac{(N+2)\,T^\star}{N} \\ &\vdots \\ t_1^{co} &= \frac{(N-1)\,T^\star}{N} + T_1^w + T_1 = \frac{(2N-1)\,T^\star}{N} \end{aligned}$$

where the right hand simplification results from the fact that $T_i + T_i^w = T^\star$. Thus, we have that $t_i^{co} - t_{i-1}^{co} = \frac{T^\star}{N}, \forall i \in \{1, ..., N-1\}$. It is straightforward to show that this holds for repeated deployments upon index wrap-around. This concludes the proof.

To simplify notation, define $f = \frac{U_{max} T^\star}{R_D}$. There exists an analytic expression for the bound on N in accordance with the conditions of this subsection.

Theorem 4 Assume that $N \geq 2$ agents are deployed one at a time with the deployment schedule and assumptions of *Remark 3*. Then:

$$N \leq \frac{\left(\frac{2}{3}\right)^{\frac{1}{3}} f^3}{\left(3^{\frac{1}{2}}\left(27f^6 - 4f^9\right)^{\frac{1}{2}} - 9f^3\right)^{\frac{1}{3}}} + \frac{\left(3^{\frac{1}{2}}\left(27f^6 - 4f^9\right)^{\frac{1}{2}} - 9f^3\right)^{\frac{1}{3}}}{2^{\frac{1}{3}}3^{\frac{2}{3}}} \quad (40)$$

is a sufficient condition such that i_{cr} enters $\mathcal{D}_{i_{cr}}$ at $t^\star \leq t^{co}_{i_{cr}}$.

Proof Take the condition:

$$N \leq \frac{\left(\frac{2}{3}\right)^{\frac{1}{3}} f^3}{\left(3^{\frac{1}{2}}\left(27f^6 - 4f^9\right)^{\frac{1}{2}} - 9f^3\right)^{\frac{1}{3}}} + \frac{\left(3^{\frac{1}{2}}\left(27f^6 - 4f^9\right)^{\frac{1}{2}} - 9f^3\right)^{\frac{1}{3}}}{2^{\frac{1}{3}}3^{\frac{2}{3}}},$$

and substitute in $g = \left(3^{\frac{1}{2}}\left(27f^6 - 4f^9\right)^{\frac{1}{2}} - 9f^3\right)^{\frac{1}{3}}$:

$$N \leq \frac{\left(\frac{2}{3}\right)^{\frac{1}{3}} f^3}{g} + \frac{g}{2^{\frac{1}{3}}3^{\frac{2}{3}}}.$$

Now find a common denominator and combine terms:

$$N \leq \frac{\left(2f^3 3^{\frac{1}{3}} + g^2 2^{\frac{1}{3}}\right) 6^{\frac{1}{3}}}{6g}. \quad (41)$$

Cubing this expression yields:

$$N^3 \leq \frac{\left(2f^3 3^{\frac{1}{3}} + g^2 2^{\frac{1}{3}}\right)^3}{36g^3} \quad (42)$$

and subtracting 1 from each side of (41) yields:

$$N - 1 \leq \frac{\left(2f^3 3^{\frac{1}{3}} + g^2 2^{\frac{1}{3}}\right) 6^{\frac{1}{3}} - 6g}{6g}. \quad (43)$$

The assumption that $N \geq 2$ produces a special case for which one may draw the following conclusion from (42) and (43):

$$\frac{N^3}{N-1} \leq \frac{\left(2f^3 3^{\frac{1}{3}} + g^2 2^{\frac{1}{3}}\right)^3}{36g^3\left(\frac{\left(2f^3 3^{\frac{1}{3}} + g^2 2^{\frac{1}{3}}\right) 6^{\frac{1}{3}} - 6g}{6g}\right)}.$$

A proof of this special case is presented in Appendix 6.3. Expanding the numerator and denominator yields:

$$\frac{N^3}{N-1} \leq \frac{24f^9 + 12f^6 g^2 3^{\frac{2}{3}} 2^{\frac{1}{3}} + 6f^3 g^4 3^{\frac{1}{3}} 2^{\frac{2}{3}} + 2g^6}{12f^3 g^2 3^{\frac{2}{3}} 2^{\frac{1}{3}} + 6g^4 3^{\frac{1}{3}} 2^{\frac{2}{3}} - 36g^3}$$

$$= f^3\left(\frac{24f^6 + 12f^3 g^2 3^{\frac{2}{3}} 2^{\frac{1}{3}} + 6g^4 3^{\frac{1}{3}} 2^{\frac{2}{3}} + \frac{2g^6}{f^3}}{12f^3 g^2 3^{\frac{2}{3}} 2^{\frac{1}{3}} + 6g^4 3^{\frac{1}{3}} 2^{\frac{2}{3}} - 36g^3}\right) \quad (44)$$

Noting common terms in the numerator and denominator, one may show that the term in parenthesis in (44) is equal to 1 if $24f^6 + \frac{2g^6}{f^3} = -36g^3$. Expanding either the left hand or the right hand side of this equation and substituting in the definition for g yields:

$$324f^3 - 36\,(3)^{\frac{1}{2}}\left(27 - 4f^3\right)^{\frac{1}{2}} f^3.$$

Therefore, (44) reduces to:

$$\frac{N^3}{N-1} \leq f^3$$

whose cubic root is:

$$\frac{N}{(N-1)^{\frac{1}{3}}} \leq \frac{U_{max}T^\star}{\bar{R}_{\mathcal{D}}}. \quad (45)$$

$\bar{R}_{\mathcal{D}}$ may be expressed in terms of $\bar{R}_{N-2}$ in the limit that $\partial\mathcal{D}_{i_{cr}} \to \mathcal{O}$. Substituting $\bar{R}_{cr} = 0$ into (33) yields:

$$V_{rem} = \frac{2}{3}\pi\bar{R}^3_{\mathcal{D}},$$

which may be substituted into (34) to yield:

$$\frac{\frac{2}{3}\pi\bar{R}^3_{\mathcal{D}}}{N-1} = \frac{2}{3}\pi\bar{R}^3_{N-2}.$$

Removing common terms and taking the cubic root of each side yields:

$$\frac{\bar{R}_{\mathcal{D}}}{(N-1)^{\frac{1}{3}}} = \bar{R}_{N-2}.$$

which may be rearranged in terms of $\bar{R}_{\mathcal{D}}$ and substituted into (45):

$$N \leq \frac{U_{max}T^\star}{\bar{R}_{N-2}}$$

which is equivalent to:

$$\bar{R}_{N-2} \leq \frac{U_{max}T^\star}{N}, \quad (46)$$

(i.e., the agent is no further away from the origin than the maximum velocity of the slowest agent multiplied by the deployment period). It is intuitive that (46) is a sufficient condition that i_{cr} may enter $\mathcal{D}_{i_{cr}}$ before $t^{co}_{i_{cr}}$. Upon selection as i_{cr}, the agent will enter Subdomain Transfer Mode and fly directly towards the origin with a velocity of U_{max} until it enters $\mathcal{D}_{i_{cr}}$. With the deployment period assumption, the agent will have a minimum remaining flight time of $\frac{T^\star}{N}$. Under the worst case scenario, the agent is at a distance $\bar{R}_{N-2}$ from the

origin at the instant before selection[1] and enters $\mathcal{D}_{i_{cr}}$ at the instant that $V_{i_{cr}} = V^{co}$. This concludes the proof.

To illustrate this bound, consider that $U_{max} = 1$ m/s, $T^\star = 1000$ seconds, $\bar{R}_\mathcal{D} = 100$ meters, and thus $f = 10$. A numerical evaluation of (40) yields an upper theoretical limit of 31 agents.

3.2 Energy-aware global coverage mode

In order to guarantee convergence of (8) to zero, we define a switched response known as Global Coverage Mode. This mode is initiated for agent i when:

$$|\hat{e}_i(t)| < \varepsilon_1. \tag{47}$$

that is, agent i's contribution to the rate of change of (8) has dropped below a predefined threshold ε_1. At this point, $\mathcal{D}$ is divided into a grid of N_c cubes $\mathcal{D}^j$, $\forall j \in \{1, ..., N_c\}$. Each $\mathcal{D}^j$ is of dimension $\sqrt{2}R_i \times \sqrt{2}R_i \times \sqrt{2}R_i$, and the possible waypoints W^j are placed at the centroid of each $\mathcal{D}^j$.These dimensions are chosen such $\mathcal{D}^j$ is inscribed within the sphere of possible orientations for $\mathcal{S}_i$. N_c shall be large enough such that the grid over-approximates the hemispherical $\mathcal{D}$. Elements of $\mathcal{D}^j$ that intersect $\partial\mathcal{D}$ shall be truncated along $\partial\mathcal{D}$ with their associated elements of W_j shifted to the new centroid.

We define the following function to encode anticipated local coverage error for agent i in each cube $\mathcal{D}^j$:

$$\hat{C}_i^j(t_{gc}) = \int_{\mathcal{D}^j} \min\{C^\star, \acute{Q}_i(t_{gc}, \tilde{p})\} d\tilde{p} + \delta\left(C^\star V_{\mathcal{D}^j} - \int_{\mathcal{D}^j} \min\{C^\star, \acute{Q}_i(t_{gc}, \tilde{p})\} d\tilde{p}\right), \tag{48}$$

where $V_{\mathcal{D}^j}$ is the volume of each $\mathcal{D}^j$ and t_{gc} is the time at which global coverage mode was initiated. (48) is the coverage weight of each cube $\mathcal{D}^j$ and is defined as ∞ if the coverage level reaches at least $C^\star$ on every point in $\mathcal{D}^j$. This is accomplished with a dirac delta function which ensures that fully covered cubes shall not be selected as waypoints. The arguments of the minimum functions prevent discrete points covered well beyond $C^\star$ from carrying an unwarranted weight. Such a scenario may result in patches of gross coverage levels producing cube coverage levels in excess of $C^\star V_{\mathcal{D}^j}$ while discrete points $\tilde{p} \in \mathcal{D}^j$ remain uncovered.

Power conservation may be encoded into the global coverage strategy by considering the relative distances of W^j from the agent. Define the actuation accumulation function:

$$\Gamma_i(t_{gc}) = \int_0^{t_{gc}} \gamma_{i1}|u_i(\tau)| + \gamma_{i2}|v_i(\tau)| + \gamma_{i3}|w_i(\tau)| + \gamma_{i4}|s_i(\tau)| d\tau \tag{49}$$

which represents the net accumulated actuator effort since deployment. $\gamma_{ik} > 0 \mid k \in \{1, ..., 4\}$ are cost weights that can be assigned based upon a particular system's rate of energy usage. (48) and (49) can be combined into the overall cost definition:

$$\tilde{j} = \arg\min_j \left((\Lambda_{i0} + \Gamma_i(t_{gc})) \|p_i - W^j\| + \Lambda_{i1} \hat{C}_i^j \right), \tag{50a}$$

$$p_{\star,i} = W^{\tilde{j}}, \tag{50b}$$

where the chosen waypoint, $p_{\star,i}$, for agent i is assigned to be the centroid of the cube indexed by $\tilde{j}$, that minimizes the cost function (50a). $\Lambda_{i0} > 0$ and $\Lambda_{i1} > 0$ are cost weights.

The cost function utilizes a static weight, Λ_{i0}, and a dynamic weight, $\Gamma_i(t_{gc})$, to penalize the selection of waypoints that are spatially distant from the agent's current position. $\Gamma_i(t_{gc})$ grows in time as a function of agent i's actuation effort. This cost is weighted against the relative coverage level of the cube. In real world implementation, the value of Λ_{i0} would be assigned upon deployment as a function of agent i's remaining battery life. This offers energy conserving flexibility to scenarios in which a multi-agent sensing network may be deployed with short notice and disparate battery charge levels. Additionally, $\gamma_{ik} \mid k \in \{1, ..., 4\}$ may be increased for individual agents which consume energy at a faster rate. These weights allow for agents with a history of less actuation effort to select more distant waypoints thus reducing the need for persistent spatial relocation of the more power constrained agents.

Upon selecting the waypoint, the agent must determine the optimal orientation to assume at the destination. This orientation will be the one for which $\mathcal{S}_i$ is exposed to the least covered subspace of $\mathcal{D}$. This can be expressed as finding the value of Ψ_i that maximizes the argument of this problem:

$$\Psi_{\star,i} = \arg\max_\Psi \left(\int_D h'\left(C^\star - \acute{Q}_i(t_{gc}, \tilde{p})\right) \left(S_i(\tilde{q}_{\star,i}, \tilde{p})\right) d\tilde{p} \right), \tag{51}$$

where $\tilde{q}_{\star,i} = \left[{p_{\star,i}}^T\, 0\, 0\, \Psi_{\star,i}\right]^T$. Selecting a destination orientation with the minimum coverage level maximizes

[1] Under the constraint of (34), $\bar{R}_\mathcal{D} > \bar{R}_1 > ... > \bar{R}_{cr} \implies \bar{R}_{N-2} - \bar{R}_{cr} > \bar{R}_{N-3} - \bar{R}_{N-2} > ... > \bar{R}_\mathcal{D} - \bar{R}_1$. The time allocated for subdomain transfer is bounded by $\frac{T^\star}{N}$ for all agents and each shell is thinner than the previous as one moves out from $\mathcal{O}$. As *Theorem 4* establishes that i_{cr} may enter $D_{i_{cr}}$ so long as it was inside of $\mathcal{D}_{N-1}$ when selected by (27), one may see that the guarantee is met recursively so long as $i = 1$ is within $\mathcal{D}$.

(12). This maximizes the initial coverage rate when local coverage mode is resumed.

Convergence to the desired position, $p_{\star,i}$, as well as collision avoidance are achieved using the following control scheme which is derived from that first presented in Panagou et al (2016) and later in Ma et al (2016). Define a nominal Lyapunov-like function:

$$\mathcal{V}_{i0} = \|p_i - p_{\star,i}\|^2. \tag{52}$$

which is positive definite and encodes convergence of agent i to the destination. Now define a global avoidance constraint for each of the $j \neq i$ friendly agents:

$$c_{4ij} = (x_i - x_j)^2 + (y_i - y_j)^2 + (z_i - z_j)^2 - (\text{ɾ}_i + \text{ɾ}_j)^2 > 0,$$

to encode that collision avoidance requires $\|p_i - p_j\| > \text{ɾ}_i + \text{ɾ}_j$. Define a logarithmic barrier function in terms of this constraint:

$$b_{ij}(p_i, p_j) = -\ln(c_{4ij}(p_i, p_j)),$$

and define, as in Wills and Heath (2002), the recentered barrier function which tends to $+\infty$ as $\|p_i - p_j\| \to \text{ɾ}_i + \text{ɾ}_j$ and zero as $p_i \to p_{\star,i}$:

$$q_{ij}(p_i, p_j) = b_{ij}(p_i, p_j) - b_{ij}(p_{\star,i}, p_j). \tag{53}$$

To ensure that our Lyapunov-like function shall ultimately be non-negative everywhere, define:

$$\mathcal{V}'_{ij}(p_i, p_j) = (q_{ij}(p_i, p_j))^2.$$

The global avoidance constraint is activated under the condition that $\|p_i - p_j\| \leq R_i$ using a bump function which is $\mathcal{C}^2$ with respect to the agent distance:

$$\sigma_{ij} = \begin{cases} 1 & \text{if } \text{ɾ}_i + \text{ɾ}_j \leq d_{ij} \leq R_z \\ Ad_{ij}^3 + Bd_{ij}^2 + Cd_{ij} + D & \text{if } R_z < d_{ij} < R_i \\ 0 & \text{if } d_{ij} \geq R_i \end{cases}$$

where $d_{ij} = \|p_i - p_j\|$ and R_z determines the steepness of the bump and is chosen such that $\text{ɾ}_i + \text{ɾ}_j < R_z < R_i$. The coefficients are defined as follows: $A = -(2/(R_z - R_i)^3)$, $B = (3(R_z + R_i)/(R_z - R_i)^3)$, $C = (-6R_zR_i/(R_z - R_i)^3)$, and $D = (R_i^2(3R_z - R_i)/(R_z - R_i)^3)$. Therefore, the global avoidance constituent Lyapunov-like function is:

$$\mathcal{V}_{ij}(p_i, p_j) = \sigma_{ij}\mathcal{V}'_{ij}(p_i, p_j),$$

which augments the nominal Lyapunov-like function:

$$\nu_i = \mathcal{V}_{i0} + \sum_{j=1}^{N-1} \mathcal{V}_{ij}$$

and may be scaled between zero and one to form our candidate Lyapunov-like function for p_i:

$$\mathcal{V}_i = \frac{\nu_i}{1 + \nu_i}. \tag{54}$$

As discussed in Ma et al (2016), trajectories that follow the negative gradient of $\mathcal{V}_i$ shall be stabilizing and in-fact almost certainly globally asymptotically stabilizing. Such a controller may be defined as:

$$\begin{bmatrix} u_i^{glo} \\ v_i^{glo} \\ w_i^{glo} \end{bmatrix} = \mathcal{R}_1^{-1} \begin{bmatrix} \frac{-\partial \mathcal{V}_i}{\partial x_i} \left(\frac{U_{max}}{\sqrt{\left(\frac{\partial \mathcal{V}_i}{\partial x_i}\right)^2 + \left(\frac{\partial \mathcal{V}_i}{\partial y_i}\right)^2 + \left(\frac{\partial \mathcal{V}_i}{\partial z_i}\right)^2}} \right) \\ \frac{-\partial \mathcal{V}_i}{\partial y_i} \left(\frac{U_{max}}{\sqrt{\left(\frac{\partial \mathcal{V}_i}{\partial x_i}\right)^2 + \left(\frac{\partial \mathcal{V}_i}{\partial y_i}\right)^2 + \left(\frac{\partial \mathcal{V}_i}{\partial z_i}\right)^2}} \right) \\ \frac{-\partial \mathcal{V}_i}{\partial z_i} \left(\frac{U_{max}}{\sqrt{\left(\frac{\partial \mathcal{V}_i}{\partial x_i}\right)^2 + \left(\frac{\partial \mathcal{V}_i}{\partial y_i}\right)^2 + \left(\frac{\partial \mathcal{V}_i}{\partial z_i}\right)^2}} \right) \end{bmatrix}. \tag{55}$$

With the exception of local coverage, whose avoidance strategies are presented in *Theorem 1*, all hybrid modes controlling linear velocity are based upon waypoints and incorporate controllers similar to (55) These modes nominally incorporate collision avoidance using logarithmic barrier functions. The anomalous scenario in which multiple agents become isolated in critical points of $\mathcal{V}_i$, a highly improbable alignment, may be overcome by defining an event in which the motion of multiple agents in the global coverage mode has halted for a predefined period of time. In this scenario, agents in local coverage should switch into global coverage mode and then the network may apply the high-level prioritized path planning protocol that is presented in Ma et al (2016). This technique is suited for high-density operations in cluttered environments. For further analysis on collision avoidance with logarithmic barriers, please see Ma et al (2016). See also, Panagou et al (2016).

Convergence to the desired orientation, $\Psi_{\star,i}$, is straightforward. For our purposes, a proportional controller was sufficient:

$$s_i^{glo} = \mathcal{R}_{2_{3,3}}^{-1} (\Psi_{\star,i} - \Psi_i) \tag{56}$$

Thus, upon computation of (50b) and (51), control laws (55) and (56) are simultaneously activated. Upon acquisition of the desired position and orientation, control shall be handed back to either local coverage mode, upon satisfaction of $G(\zeta_{i1}, \zeta_{i0}$, or Waypoint Scan Mode, upon satisfaction of $G(\zeta_{i1}, \zeta_{i3})$. If at any time i lies outside of the intended operating range, as consistent with $G(\zeta_{i1}, \zeta_{i2}$, control is handed to Subdomain Transfer Mode.

3.3 Subdomain transfer mode

In Sect. 3.1.3, it was demonstrated that the power constrained operational safety requirement of Sect. 2.2 is met so long as $p_{i_{cr}} \in \mathcal{D}_{i_{cr}}$ in the limit that $t \to t^{co}_{i_{cr}}$. and similarly that $p_{i_\ell} \in \mathcal{D}_{i_\ell}$, $\forall \ell \in \{1, ..., N-1\}$ in the limit that $t \to t^{co}_{i_{cr}}$. These guarantees are met with subdomain transfer mode as described earlier in *Theorem 4* and *Footnote 1*.

This mode may be entered into from any of the other modes as triggered by the equivalent conditions $G(\zeta_{ik}, \zeta_{i2})$, $\forall k \in \{0, 1, 3, 4\}$. The linear velocity control law of this mode shall be denoted as: $[u_i^{sub}\, v_i^{sub}\, w_i^{sub}]^T$, and is equal to the right hand side of (55) with $p_{\star,i} = \mathcal{O}$. The angular velocity control law of this mode shall be denoted as s_i^{sub} and is equal to the right hand side of (56) with:

$$\Psi_{\star,i} = \arctan 2\left(\frac{-y_i}{\sqrt{x_i^2 + y_i^2 + z_i^2}}, \frac{-x_i}{\sqrt{x_i^2 + y_i^2 + z_i^2}}\right). \quad (57)$$

With this choice of $\Psi_{\star,i}$, agent i aims to align the $\hat{x}_{\mathcal{B}_i}$ axis, the center line of $\mathcal{S}_i$, with the xy-plane projection of $-p_i$ during subdomain transfer. This orients $\mathcal{S}_i$ to be inward looking towards the origin thus ensuring that $\mathcal{S}_i$ will be inside of the target subdomain when control is handed to local coverage mode.

3.4 Waypoint scan mode

For $G(\zeta_{i1}, \zeta_{i3})$ to be satisfied, the cube $\mathcal{D}^j$ will contain space that has not yet been fully covered. However, the $|\hat{e}_i(t)|$ is not large enough to warrant exploration in local coverage mode. Such a situation often occurs in practice when there is uncovered space within $\mathcal{D}^j$ directly above or below the agent while $\|p_i - p_{\star,i}\| < \varepsilon_2$ is satisfied. Under these conditions, no choice of Ψ_i will bring this portion of space inside of $\mathcal{S}_i$. One solution is to design a hybrid mode in which the agents patrol a defined path within $\mathcal{D}^j$ until the cube has been fully swept over.

An intuitive solution would be for the agent to select sub-waypoints above and below $W^{\tilde{j}}$ and to yaw through one complete revolution at each sub-waypoint. However, as Fig. 5 (a) illustrates, this path would contain gaps in the sweep due to the spherical sector shape of $\mathcal{S}_i$. Through symmetry, it is clear that the angle of the horizontal vertices of the gaps is 2α. The sub-waypoints illustrated in Fig. 5 (b) are placed at these vertices to allow for the gaps to be swept over. Only the left half sweep is illustrated in order to avoid clutter. A total of 13 sub-waypoints may be positioned as shown in Fig. 6 relative to $W^{\tilde{j}}$ to guarantee that $\mathcal{S}_i$ sweeps over all $\tilde{p} \in \mathcal{D}^j$. This holds true even for $\tilde{p}$ outside of the cross-section of Fig. 5 so long as $\frac{\pi}{4} \leq \alpha < \frac{\pi}{2}$. This is verified in *Theorem 5*.

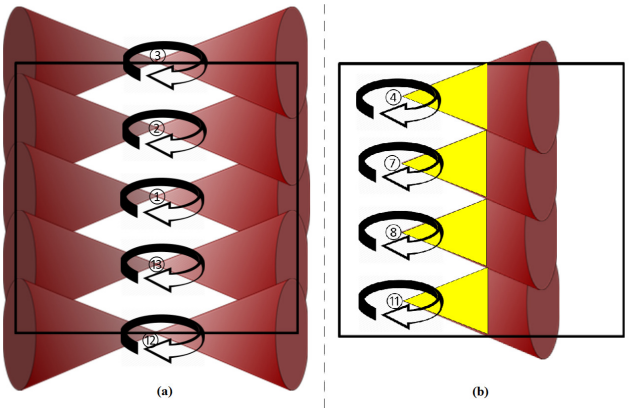

Fig. 5 Sub-waypoints directly above or below $W^{\tilde{j}}$ will leave to coverage gaps in (a). Additional points positioned laterally guarantee coverage of the left half of the gaps in (b).

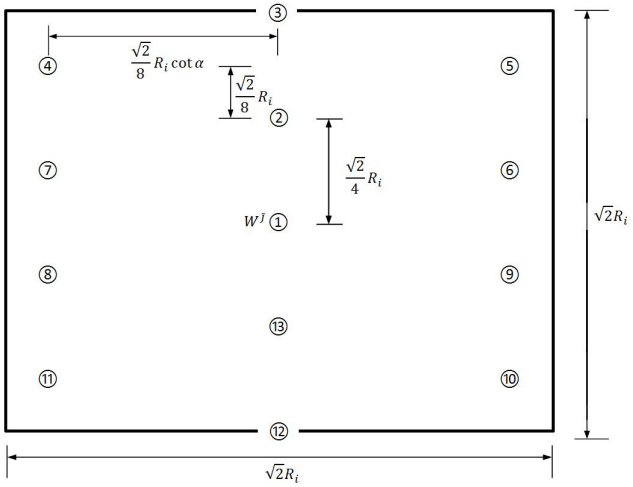

Fig. 6 In Waypoint Scan Mode, agent i will travel between 13 sub-waypoints whose position relative to $W^{\tilde{j}}$ is defined here.

Theorem 5 If agent i yaws through a complete revolution at each of the 13 sub-waypoints illustrated in Fig. 6, a vertical plane bisecting $\mathcal{D}^j$, then $\mathcal{S}_i$ shall sweep over all $\tilde{p} \in \mathcal{D}^j$ so long as $\frac{\pi}{4} \leq \alpha < \frac{\pi}{2}$.

Proof Revolutions of $\mathcal{S}_i$ about sub-waypoints above and below $W^{\tilde{j}}$ will produce four coverage gaps as illustrated in white in Fig. 5 (a). Each of these gaps may be represented in 3-D space by two cones, of radius $\frac{\sqrt{2}}{8} R_i \cot\alpha$ and height $\frac{\sqrt{2}}{8} R_i$, whose planar surfaces are coincident. It shall be shown that a yaw revolution of i at sub-

waypoint 4 sweeps $\mathcal{S}_i$ across all $\tilde{p}$ in the left half of the top coverage gap as indicated in yellow in Fig. 6 (b).

This left-side gap is again indicated in yellow and projected into 3 orthogonal planes: front (a), side (b), and top (c) in Fig. 7. These projections shall be referenced throughout the remainder of this proof. The geometry of coverage gap projection (a), whose left-side vertex has angle 2α, may be fully contained within $\mathcal{S}_i$ at the illustrated yaw orientation so long as $\frac{\sqrt{2}}{8}R_i \cot\alpha \leq R_i$ which is equivalent to the condition that $\tan\alpha \geq \frac{\sqrt{2}}{8}$.

Gap projection (b) is obtained from the 90° right-handed rotation indicated in (a). The vertical height of gap projection (b) equal to that of the diameter of $\mathcal{S}_i$ within this plane by virtue of the above-stated gap vertex angle 2α. The horizontal width of gap projection (b) shall not extend outside of $\mathcal{S}_i$ so long as $\frac{\sqrt{2}}{8}R_i \cot\alpha \leq \frac{\sqrt{2}}{8}R_i$ which is equivalent to the condition that $\tan\alpha \geq 1$.

Gap projection (c) is obtained from the 90° right-handed rotation indicated in (b) and is a semicircle. Agent i's 360° yaw motion about sub-waypoint 4 shall sweep across this semicircle so long as R_i is greater than or equal to the indicated chord length $\frac{1}{4}R_i \cot\alpha$ which is equivalent to the condition that $\tan\alpha \geq \frac{1}{4}$. The inequality constraints on $\tan\alpha$ are all satisfied when $\frac{\pi}{4} \leq \alpha < \frac{\pi}{2}$. Under this condition, a full yaw revolution of i shall sweep $\mathcal{S}_i$ over all points of the three orthonormal coverage gap projections indicated in Fig. 7 and thus over all points of the coverage gap. Through symmetry it may be shown that sub-waypoints 5-11 sweep over all remaining $\tilde{p}$ in coverage gaps. Thus, $\mathcal{S}_i$ sweeps over all $\tilde{p} \in \mathcal{D}^j$. This concludes the proof.

Recall from Sect. 2.3 that these 13 sub-waypoints are indexed by wp and note that this is to be done in a manner consistent with Fig. 6. The automaton defined in Sect. 2.3 calls for an input $f(\zeta_{i3}, \tilde{q}_i)$ to transition between sub-waypoints and an input $f(\zeta_{i4}, \tilde{q}_i)$ for the 360° revolution at each sub-waypoint. $[u_i^{wps}\ v_i^{wps}\ w_i^{wps}]^T$ is equal to the right hand side of (55) with $p_{\star,i}$ equal to the element of the set of points defined in Fig. 6 with index wps. s_i^{wps} is equal to an arbitrary positive constant. $G(\zeta_{i3}, \zeta_{i4})$ provides a definition for sub-waypoint capture consistent with this work and $G(\zeta_{i4}, \zeta_{i3})$ is satisfied upon completion of one revolution–that is, an arbitrary positive s_i^{wps} command has rotated i to an orientation $\Psi_i = \Psi_i(t_{G(\zeta_{i3},\zeta_{i4})}) - d\Psi$.

3.5 Theoretical Coverage Guarantee

Theorem 6 The control strategy defined above guarantees that the global coverage error $E(t)$ shall be driven to zero.

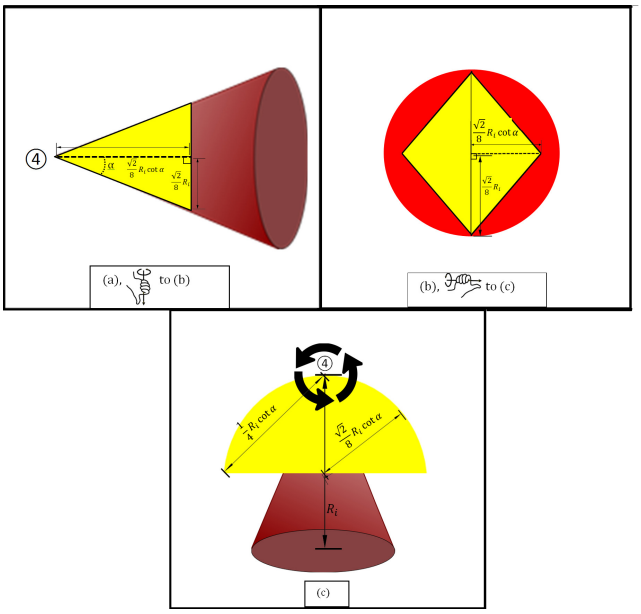

Fig. 7 The coverage gap resulting from sweeps at sub-waypoints 2 and 3 is indicated in yellow and projected into 3 orthogonal planes in (a), (b), and (c). View (a) is the same as Fig. 6 and subsequent views are indicated by right hand rotations on the figure.

Proof As the protocol approaches complete coverage, if one may upper-bound $\dot{E}(t) < 0$ then convergence of $E(t)$ to zero is trivial. In reality, i's contribution to $\dot{E}(t)$, i.e. $\hat{e}_i$, shall tend to maintain an absolute value less than ε_1. With $G(\zeta_{i0}, \zeta_{i1})$ and $G(\zeta_{i1}, \zeta_{i3})$ persistently satisfied for agent i operating within it's prescribed subdomain, the agent shall repeatedly trigger waypoint scan mode. The geometry of the sub-waypoints within each cube $\mathcal{D}^j$ guarantee that waypoint scan mode shall cover all of $\mathcal{D}^j$ given a sufficient number of activations as verified in *Theorem 5*. Global coverage mode shall continue to select new $\mathcal{D}^j$, $\forall j \in \{1, ..., N_c\}$ and hand over coverage to waypoint scan mode until the entire domain has been sufficiently covered. Thus, the coverage error shall converge to zero. This concludes the proof.

4 Experimental and Simulation-based Verification

4.1 Experimental Procedure

The coverage strategy was validated experimentally in an indoor test environment with the agents dispatched to explore a 2.55 m x 2.55 m x 2.3 m box. We used three commercially available Hummingbird quadrotors manufactured by Ascending Technologies. These vehicles each powered by a single 11.1 Volt lithium polymer battery nominally rated at 2100 mAh. Each quadrotor features two embedded processors running at 1 kHz,

denoted as the high-level processor (HLP) and the low-level processor (LLP). Additionally, our ground station is a Dell Inspiron 3847 Desktop running Ubuntu 14.04 LTS on an Intel Core i7-4790 CPU @ 3.80 GHz x 8 with 15.6 GB of RAM. Attitude and position measurements for each quadrotor are provided by a Vicon motion capture system. The system runs at 250 Hz and provides accurate position measurements to within 1 mm within our test section.

The Robot Operating System (ROS) provides a framework for exchanging data between the ground computer station, Vicon system, and the quadrotors. The control algorithm, as presented, is implemented in MATLAB. The resultant velocity inputs are transmitted via XBee serial modules from the ground station to the HLP through ROS using the Robotics System Toolbox. The HLP then issues motor commands to the LLP for execution. The desired rotor rates are achieved through the embedded proprietary control software in the LLP.

The cutoff voltage, V^{co}, was chosen as 10 Volts as this guaranteed an additional 30 seconds or so of flight time for the Hummingbirds to transition from a hovering state through a stable landing sequence. After selecting this value, discharge trends of six batteries were recorded for a single agent trial in-order to determine an appropriate value for the parameter $T^{\star}$. These trends are presented in Fig. 8. The discharge times, denoted earlier as T_i, for the six batteries were 743, 758, 759, 755, 786, and 563 seconds respectively. $T^{\star}$ was chosen to be 990 seconds as this provides an upper bound on the measured discharge times and provides a sufficient window to install a fresh battery and re-establish communication with the ground station.

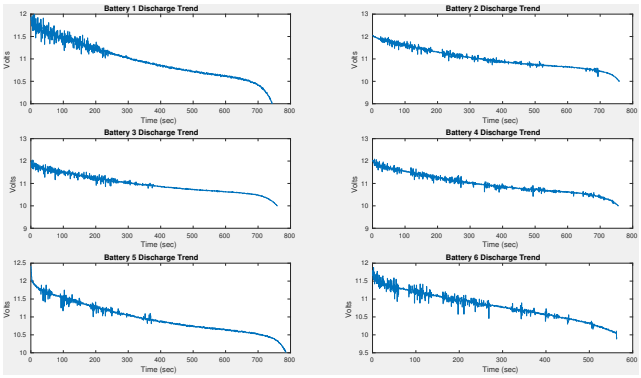

Fig. 8 T_i values were experimentally determined for six batteries. These values are 743, 758, 759, 755, 786, and 563 seconds respectively.

Within our MATLAB code, the parameter $Q(t, \tilde{p})$ is represented by a large 3D matrix. This matrix is called each time step and augmented with the parameters $M_{1i}(p_j, \tilde{p})$, $\forall i \in \{1, ..., N\}$, $M_{2i_{cr}}(t, \tilde{p})$, and $M_{3\ell}(p_j, \tilde{p})$, $\forall l \in \{1, ..., N-1\}$. Thus, it is required that specific regions of $Q(t, \tilde{p})$ be accessed by their index locations and set to $C^{\star}$ each time step. Although this work nominally describes the shapes of these augmentation functions as spherical or hemispherical, an infinity norm may be equivalently used in their definitions rather than the implicit Euclidean norm. The infinity norm was chosen for our experimental implementation as it allowed for the augmentation functions to be defined in terms of a set of cuboid regions whose boundaries correspond in a direct manner to large index ranges. This allowed for vectorization based code which MATLAB is optimized to process. For this reason our experimental domain is a cuboid rather than a hemisphere.

Two trials were conducted with identical parameter values. In each trial, one of the three agents was deployed from the origin every 5 minutes and 30 seconds nominally and tasked to explore the environment. The six batteries mentioned above were utilized in sequential order such that each agent should have two active exploration periods. As $V_i(t)$ of agent i approaches V^{co}, the quadrotor's position would converge upon the origin and hover a few inches above the ground. When the target position had been acquired and the battery voltage had dropped below V^{co}, an operator would cut off power to the motors thus dropping the quadrotor to the ground at it's current lateral position. The operator would then walk into the test section while avoiding the active quadrotors and replace the battery during the waiting period, T_i^w. At the next deployment point, t_i^d, the operator would return power to the agent and immediately hand control back to the ground station. With this protocol, the domain was persistently explored for upwards of 40 minutes with 2-3 quadrotors continuously in the air after the second deployment window. It should be noted here that in both trials 80% coverage was achieved within the first 10 minutes, the trials were permitted to run for 40 minutes in order to illustrate the long term efficacy of the deployment window spacing. The parameter values for both trials are presented in Table 1.

4.2 Experimental Results and Discussion

The coverage error evolution and inter-agent distances are presented in Figs. 9 and 10 respectively. It should be noted that the plotted value for $\hat{r}_i + \hat{r}_j$ is a physical measurement of 0.51 meters. The true value implemented in the MATLAB controller was set to 0.64 m in order to allow for some margin of stopping space on the part of the Ascending Technologies low level controller. Our use of second-order modelling necessitates this margin

Table 1 The following parameter values were used in both trials

Parameter	Value	Parameter	Value
$C^\star$	10	$T^\star$	5 min 30 sec
k_u^{loc}	5×10^{-8}	k_v^{loc}	5×10^{-8}
k_w^{loc}	5×10^{-8}	k_s^{loc}	1×10^{-7}
ε_1	3.7 Hz	ε_2	0.2 m
ε_3	0.3 rad	U_{max}	0.1 m/s
$\kappa_{i_{cr}}$	0.13 m/V	$\gamma_{ik}, \forall k \in \{1, ..., 4\}$	7.8×10^{-3}
Λ_{i0}	40	Λ_{i1}	2.7×10^5
R_i	0.64 m	α	60°

as the vehicles cannot instantaneously change direction when new kinematic commands are uploaded.

For trial one, 50%, 80%, and 90% coverage were achieved after 236, 463, and 1241 seconds respectively. The protocol terminated with 95.6% coverage at 2350 seconds. Two anomalies occurred during this run. The first anomaly occurred at 1669 seconds. Fig. 9 illustrates that the proximity of agents 2 to 3 comes within a few centimeters less than $\mathscr{z}_i + \mathscr{z}_j$ at this time and yet the agents do not collide. At this moment, agent 2 was flying directly above agent 3 thus placing agent 3 into a downdraft generating additional control action and ultimately overcompensation on the part of the low level controller. This caused no issues as the vertical dimensions of the quadrotors are substantially less than the lateral dimensions. In future trials, the effect could be compensated for by increasing our margin for $\mathscr{z}_i$. Furthermore, this effect shall be eliminated in our future work which shall implement quadrotor dynamics-based coverage control strategies rather than relying upon proprietary low level controllers such as those developed by Ascending Technologies. The second anomaly occurred at 1572 seconds. After agent 1's redeployment at 995 seconds, it proceeded to operate correctly until a communication failure in the Xbee links occurred at 1572 seconds resulting in the agent flying out of control into our safety net thus ceasing coverage earlier than intended. The two remaining agents continued covering until the expiration of their batteries. As Table 2 illustrates, all six deployment windows occurred within 5 seconds of their nominal times and aside from the communication failure crash, all other exploration periods ended with a successfully executed landing at the origin. A video of trial one is available at `https://www.youtube.com/watch?v=UjDi9PYa0zY&t=107s`.

For trial two, 50%, 80%, and 90% coverage were achieved after 211, 511, and 856 seconds respectively. The protocol terminated with 97.4% coverage at 1859 seconds. Anomalies not associated with the algorithm itself occurred during this run. Specifically, another Xbee communication failure occurred at 1818 seconds leading to the crash of Agent 2 during it's second exploration protocol. Agent 3 was then landed manually 41 seconds later in order to assess damage to the crashed quadrotor. As Table 3 illustates, five of the deployment windows occurred within seconds of the nominal times; however, agent 3 was relaunched 30 seconds early due to human error.

Table 2 For trial one, the nominal and true launch times are presented as well as the true landing times. Time is presented in seconds

Agent	Nominal Launch	True Launch	Landing
1	0	2	692
2	330	333	1211
3	660	663	1581
1	990	995	1572
2	1320	1322	2250
3	1650	1653	2360

Table 3 For trial two, the nominal and true launch times are presented as well as the true landing times. Time is presented in seconds

Agent	Nominal Launch	True Launch	Landing
1	0	2	690
2	330	333	1210
3	660	663	1560
1	990	993	1655
2	1320	1323	1818
3	1650	1622	1852

The battery voltage trends and operating modes of our hybrid automaton are presented for each trial in Figs. 11 and 12 respectively. The initial deployments for agent 1 in both trials are reflective of the fact that battery 1 has the shortest lifespan in the network. It was originally measured at 743 seconds in the days preceding our experiments and has further deteriorated through practice and tuning trials. However, these first deployment trends in Figs. 11 and 12 reflect that the 30 seconds of buffer time built into the choice of V_{co} still allow for the agent to converge upon $\mathcal{D}_{i_{cr}}$ which has now retracted to a point at the origin. This is essentially a compensation for the uncertainty in T_i as agents are actually able to maintain altitude with batteries readings as low as 9 Volts. Note in both of these figures that the tails of voltage trends always correspond with motion in subdomain transfer mode. The trajectories of the agents over the course of the trials are presented in Figs. 13 and 14 for reference.

Most of the anomalies reported are unrelated to the performance of the algorithm itself and result from the inevitable hardware, software and human errors that accumulate over the course of a complex 40 minute experiment. These experiments demonstrate that ap-

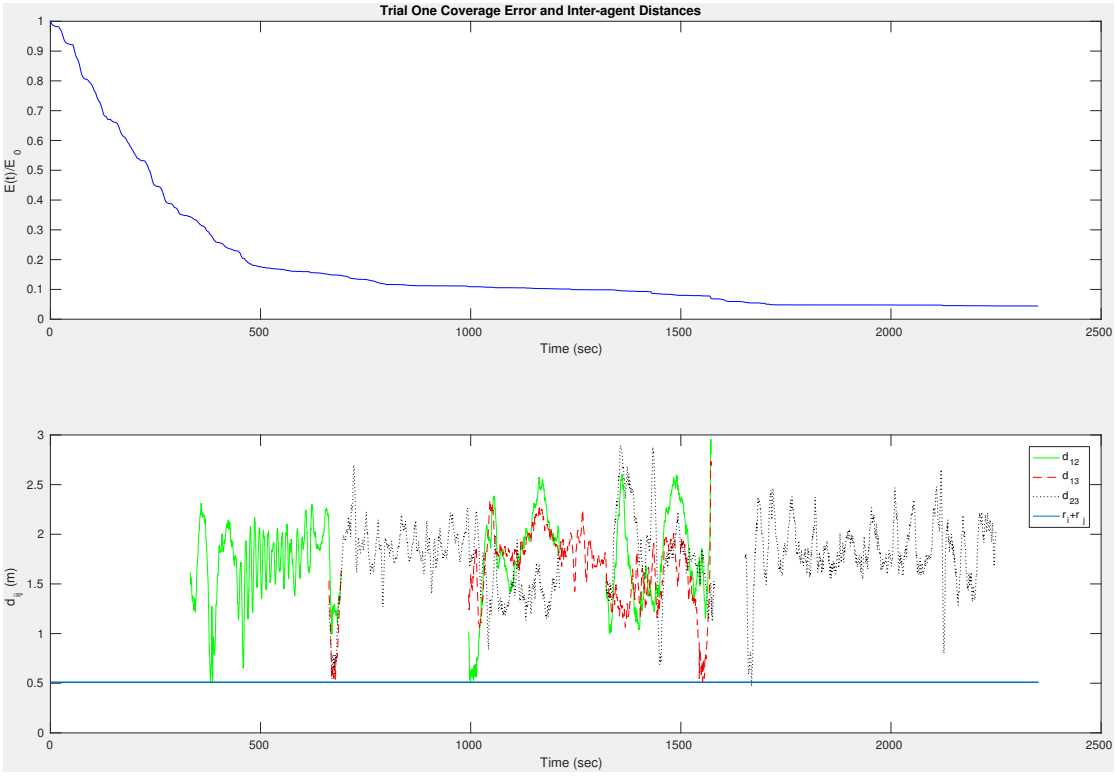

Fig. 9 For Trial One 50%, 80%, and 90% coverage were achieved after 236, 463, and 1241 seconds respectively. The protocol terminated with 95.6% coverage at 2350 seconds. The agents successfully avoided collision although a vertical anomaly occurred at 1669 seconds between agents 2 and 3. d_{ij} is the distance of agent i from agent j, and the MATLAB typeset $r_i + r_j$ is intended as the minimum safe distance ($\texttt{r}_i + \texttt{r}_j$).

propriately spaced periodic deployments of quadrotors from a single charging station can result in a long-duration surveillance operation. Additionally, our energy-aware domain partitioning technique resulted in trajectories that were globally attractive to our charging station in the limits that batteries expired. Aside from the anomalies discussed, each agent's flight path was directed to the origin as the battery expired allowing for a human to swap out the battery before the next redeployment window arrived.

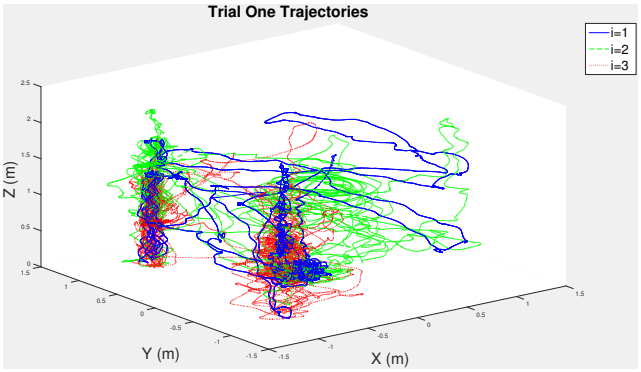

Fig. 13 The trajectories of the three agents, indexed $i = 1$, $i = 2$ and $i = 3$ respectively, are presented over the course of trial one.

4.3 Simulation

A simulation was performed with $N = 10$ agents to illustrate the scalability of the algorithm. The following parameters differ from the experimental trials: $\texttt{r}_i = 0.5$, $R_i = 10$, $k_u^{loc} = k_v^{loc} = k_w^{loc} = 0.07$, $k_s^{loc} = 0.015$, and $T^\star = T_i = 238$ seconds for all agents. 90% and 95% coverage of the domain were achieved in 4567 and 8438 seconds respectively.

For the interest of data visualization clarity, only the first 300 or 3000 seconds of coverage time are presented in simulation figures. Agents deploy every 23.8 seconds from the charging station. The coverage error and inter-agent distances are presented in Fig. 15. Only distances with respect to $i = 1$ are presented to reduce clutter; however, all agents successfully avoid collision.

Battery voltage trends for the ten agents are presented in Fig. 16. All agents use the same voltage trend: a recording of one of our lab quadrotors hovering for 5 minutes. The automaton modes for the first four agents are presented in Fig. 17 which provides the most striking contrast to that of the experimental results. Due

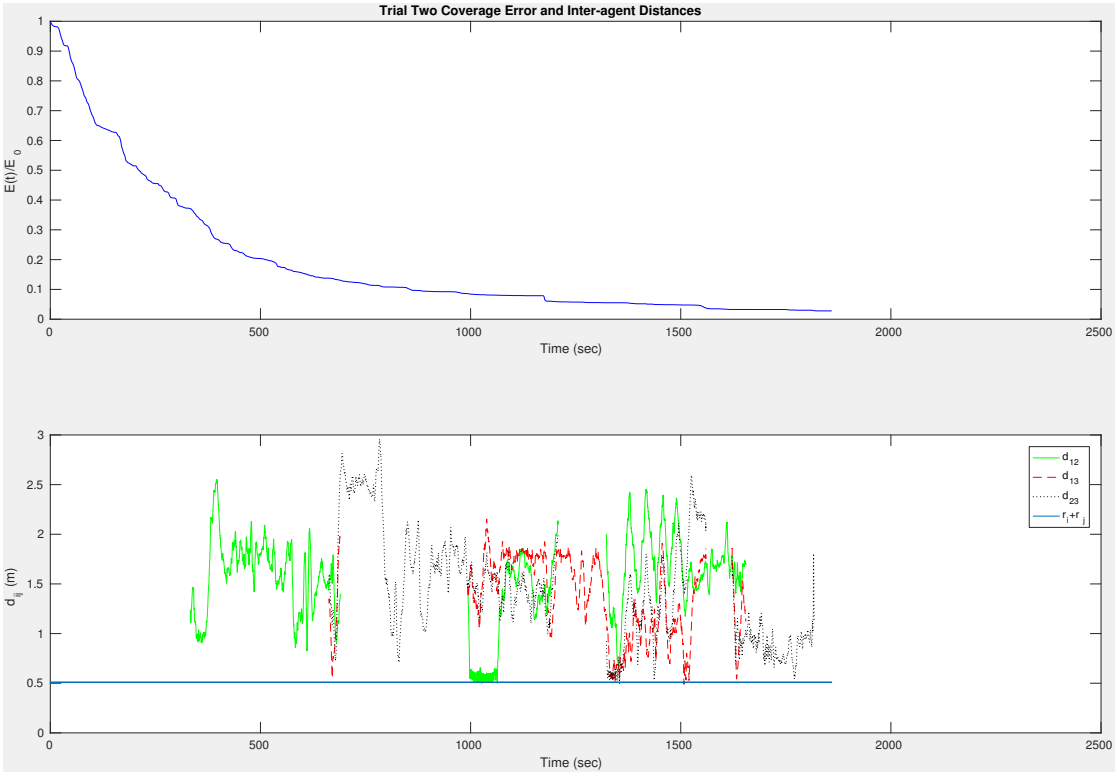

Fig. 10 For Trial Two 50%, 80%, and 90% coverage were achieved after 211, 511, and 856 seconds respectively. The protocol terminated with 97.4% coverage at 1859 seconds The agents successfully avoided collision. d_{ij} is the distance of agent i from agent j, and the MATLAB typeset $r_i + r_j$ is intended as the minimum safe distance ($\texttt{r}_i + \texttt{r}_j$).

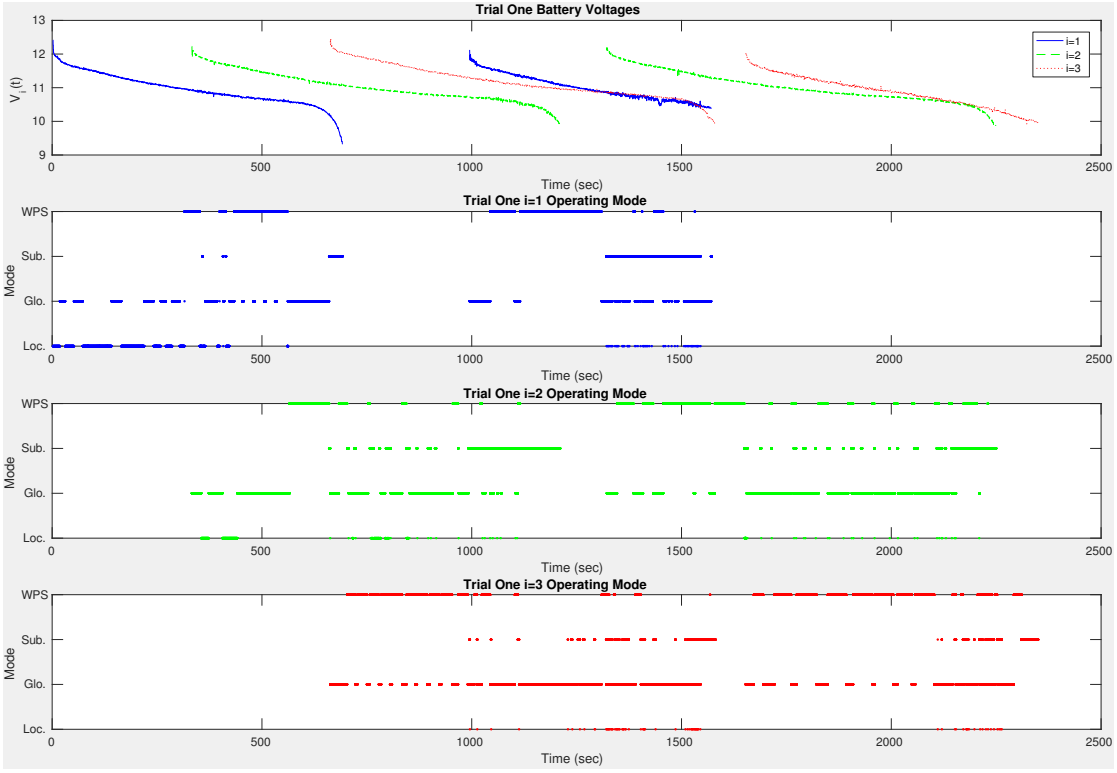

Fig. 11 The six battery trends over the course of trial two are presented as well as the automaton modes of each of the three agents indexed $i = 1$, $i = 2$ and $i = 3$ respectively.

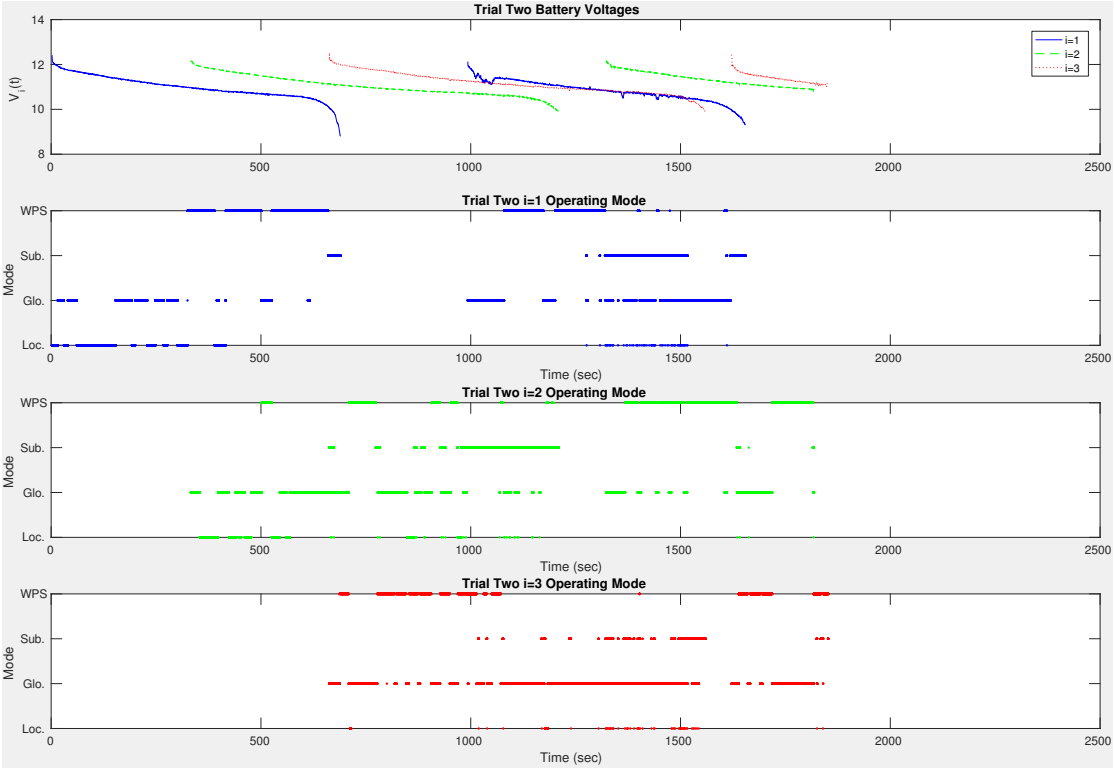

Fig. 12 The six battery trends over the course of trial two are presented as well as the automaton modes of each of the three agents indexed $i = 1$, $i = 2$ and $i = 3$ respectively.

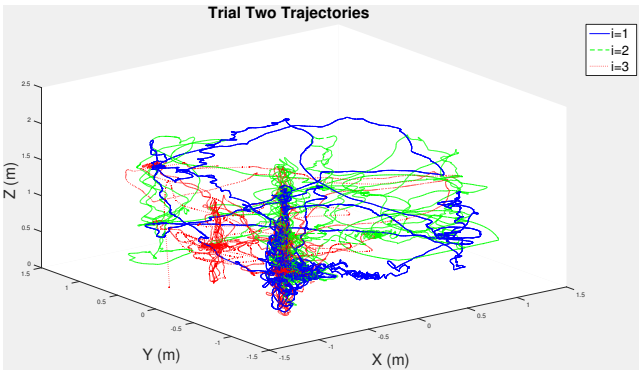

Fig. 14 The trajectories of the three agents, indexed $i = 1$, $i = 2$ and $i = 3$ respectively, are presented over the course of trial two.

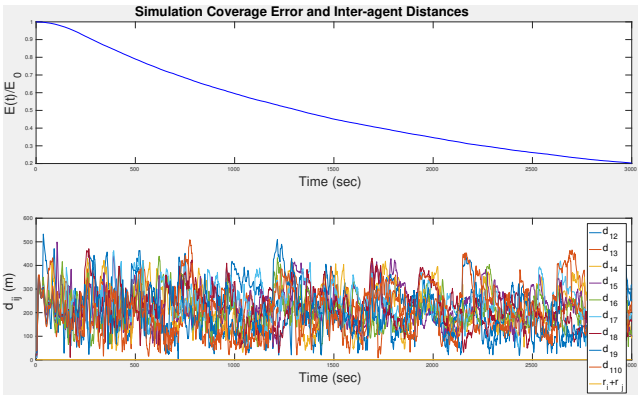

Fig. 15 All ten agents avoided collision throughout the simulation. Only $i = 1$'s proximity from each agent is presented to reduce clutter. The MATLAB typeset $r_i + r_j$ is intended as the minimum safe distance ($\mathscr{r}_i + \mathscr{r}_j$).

to the small size of our lab space, it was difficult for agents to spend much time in local coverage mode as their sensing footprints were rather large compared to the size of the space. The increased exploration volume in simulation allowed for agents to spend more time in local coverage mode.

The trajectory of agent 1 for the first 300 seconds is presented in Fig. 18. The agent deploys from the origin and then transfers to the outer shell. The exploratory trajectory gradually converges upon the origin at 238 seconds. The agent is then redeployed. Fig. 19 displays $S_i(\tilde{q}_i, \tilde{p})$ for $i \in \{1, ..., 10\}$ over various shots in time to further illustrate the deployment strategy. The anisotropic quality of $S_i(\tilde{q}_i, \tilde{p})$ is visualized in Fig. 19. The coverage level over time of a vertical cross section of the domain is presented in Fig. 20.

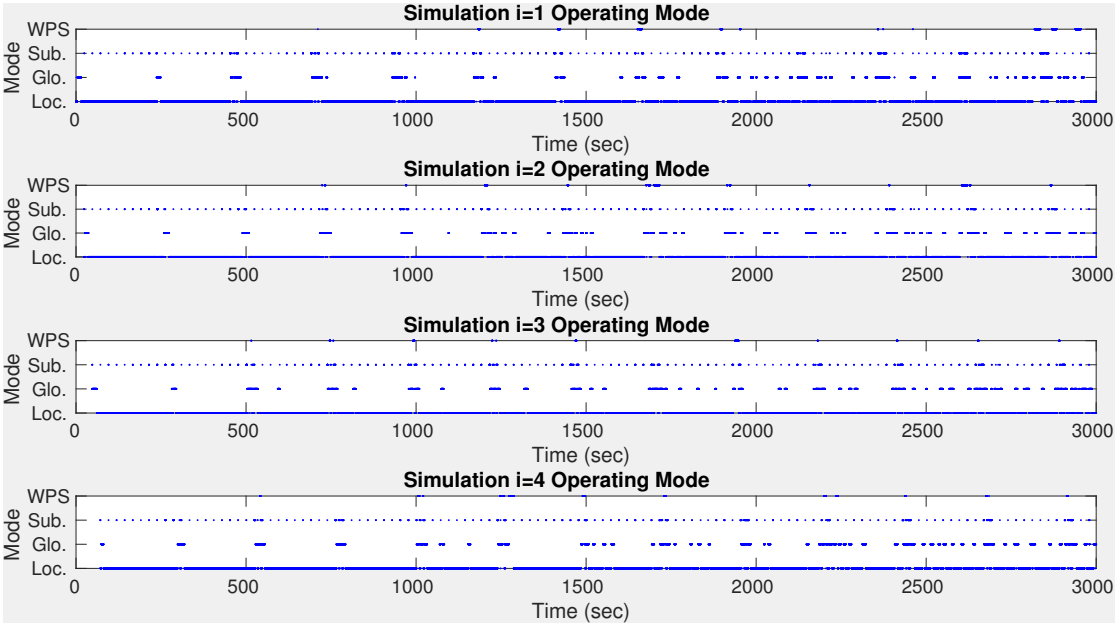

Fig. 17 Automaton modes for the first four agents are presented. Agents deploy from the charging station and transfer to their designated shells in global coverage mode. Local coverage mode guides active exploration, while short periods of subdomain transfer mode appear every 23.8 seconds to transfer agents to inner shells.

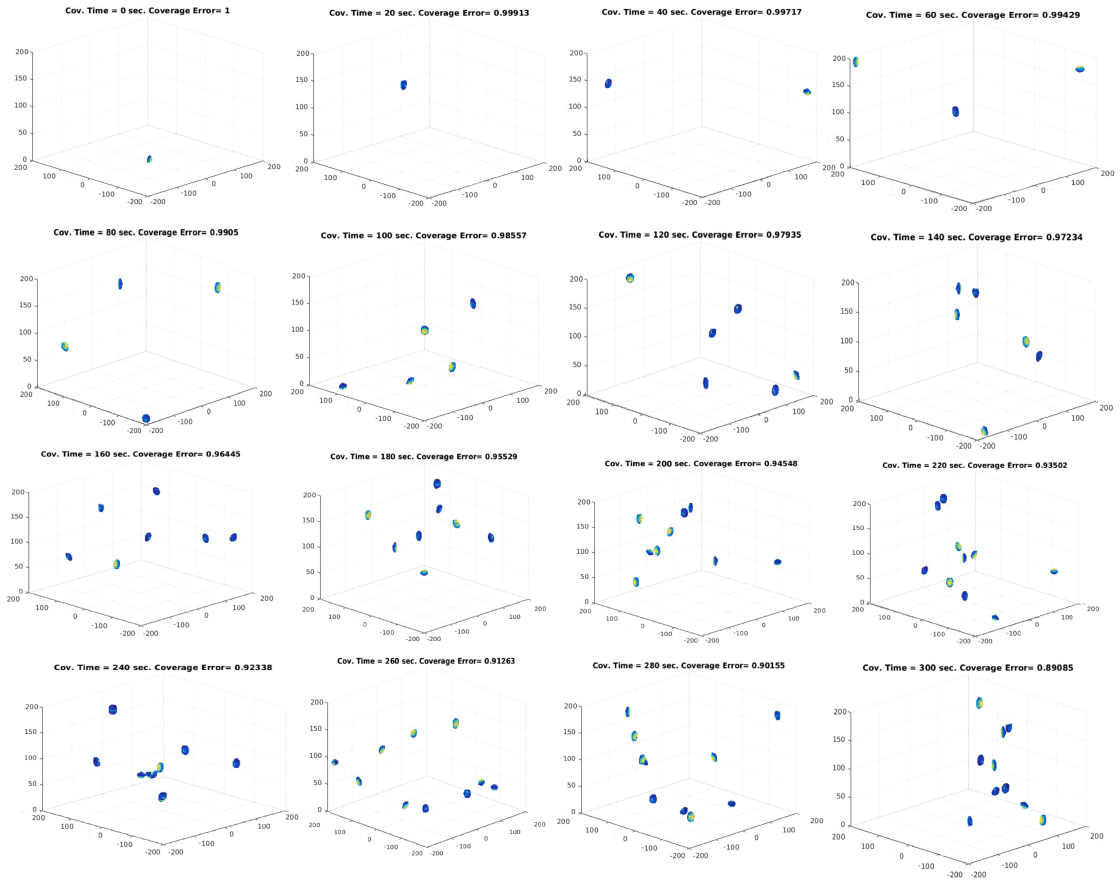

Fig. 19 The first 300 seconds of simulation time is presented with color plots of $S_i(\tilde{q}_i, \tilde{p})$ for $i \in \{1, ..., 10\}$.

5 Conclusion

This paper has presented an energy-aware 3D dynamic coverage control algorithm which extends the authors' studies in Panagou et al (2016, in press), Bentz and

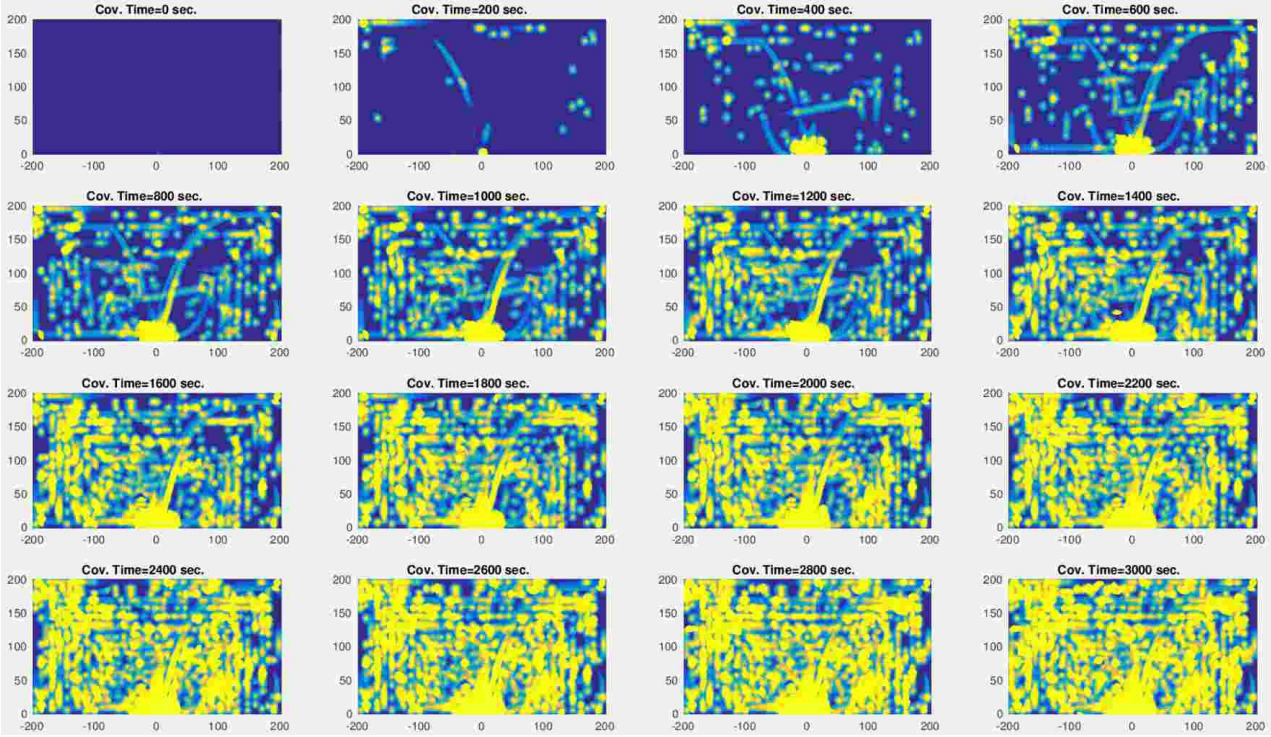

Fig. 20 The coverage level of a vertical cross section of the domain is presented for the first 3000 seconds using the standard MATLAB color scale with dark blue indicating zero coverage and bright yellow indicating a coverage level of $C^\star$.

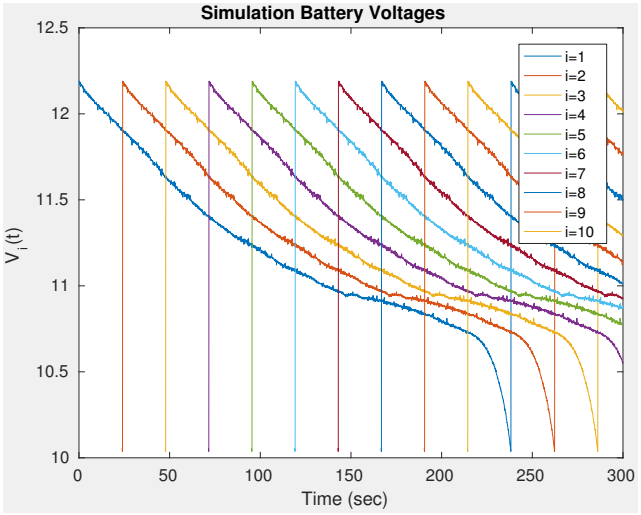

Fig. 16 Voltage for each of the ten agents is displayed during the first 300 seconds of simulation time. Agents deploy every 23.8 seconds.

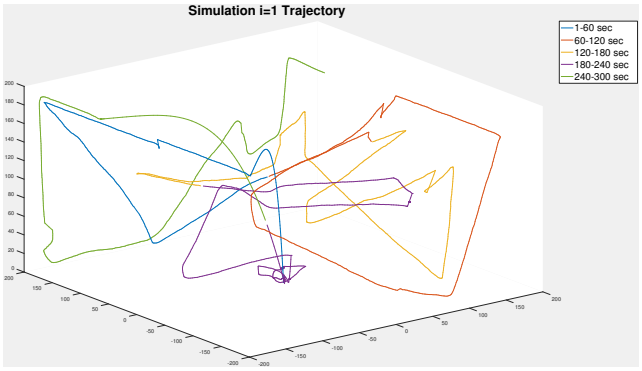

Fig. 18 The trajectory of $i = 1$ is presented for the first 300 seconds. Color is used to indicate time spans along the trajectory to aid the reader in tracing.

Panagou (2016), and Bentz and Panagou (2017) by introducing dynamic domain partitioning. This novel partitioning methodology guarantees the generation of globally attractive flight trajectories in the limit of battery expiration. This control strategy is applicable to active 3D search, patrol, and environmental monitoring protocols. Previous work on this topic has been restricted quasi-3D coverage domains (Cheng et al 2008).

The efficacy of the algorithm has been demonstrated through experiments and simulations which highlight the effectiveness of the coverage protocol while maintaining the guaranteed safety provisions.

Future work will implement coverage control techniques into dynamic models of quadrotor flight. This will allow for collision avoidance guarantees to hold under more aggressive flight patterns. Additional work will explore the use of density maps and information decay to model persistent coverage of 3D dynamic environments. Object recognition and state estimation will be an integral component of this architecture which,

when augmented with pursuit/evasion games, will result in a fully autonomous 3D search and defend protocol.

6 Appendix

6.1 Automaton

The automaton is described by the following entities (Lygeros 2004):

- a set of discrete states: $Z_i = \{\zeta_{i0}, \zeta_{i1}, \zeta_{i2}, \zeta_{i3}, \zeta_{i4}\}$ which represent local coverage, global coverage, subdomain transfer, and waypoint scan modes (1) and (2) respectively,
- a set of continuous states: $\tilde{q}_i = \{x_i, y_i, z_i, \Phi_i, \Theta_i, \Psi_i\}$ representing the position and orientation of agent i in Cartestian coordinates and 3-2-1 Euler angles respectively,
- a vector field:
  $f(\zeta_{i0}, \tilde{q}_i) = \mathcal{R}\left[\acute{u}_i^{loc}\ \acute{v}_i^{loc}\ \acute{w}_i^{loc}\ 0\ 0\ \acute{s}_i^{loc}\right]^T$,
  $f(\zeta_{i1}, \tilde{q}_i) = \mathcal{R}\left[u_i^{glo}\ v_i^{glo}\ w_i^{glo}\ 0\ 0\ s_i^{glo}\right]^T$,
  $f(\zeta_{i2}, \tilde{q}_i) = \mathcal{R}\left[u_i^{sub}\ v_i^{sub}\ w_i^{sub}\ 0\ 0\ s_i^{sub}\right]^T$,
  $f(\zeta_{i3}, \tilde{q}_i) = \mathcal{R}\left[u_i^{wps}\ v_i^{wps}\ w_i^{wps}\ 0\ 0\ 0\right]^T$,
  $f(\zeta_{i4}, \tilde{q}_i) = \mathcal{R}\left[0\ 0\ 0\ 0\ 0\ s_i^{wps}\right]^T$,
  where $\mathcal{R} = \begin{bmatrix}\mathcal{R}_1 & 0\\ 0 & \mathcal{R}_2\end{bmatrix}$ and $\dot{\tilde{q}}_i = f(\zeta_{ik}, \tilde{q}_i)$ is the control input for agent i in state ζ_{ik}. Note that ζ_{i0}, ζ_{i1} and ζ_{i2} command both translation and yaw while ζ_{i3} only commands translation and ζ_{i4} only commands yaw. This is because ζ_{i3} commands that agent i transition between the sub-waypoints of waypoint scan mode while ζ_{i4} commands the 360° yaw sweep at each sub-waypoint.
- A set of initial states:
  $\{\zeta_{i0}\} \times \{\tilde{q}_i \in \mathbb{R}^6 \mid \|p_i\| \leq \bar{R}_{\mathcal{D}} \wedge \Phi_i \in (-\pi, +\pi)$
  $\wedge\ \Theta_i \in \left(\frac{-\pi}{2}, \frac{+\pi}{2}\right) \wedge \Psi_i \in (-\pi, +\pi)\}$ encoding that each agent begin in local coverage mode inside of the domain at an orientation within the traditional Euler angle range,
- a domain:
  $Dom\left(\zeta_{i0}\right) = \{\tilde{q}_i \in \mathbb{R}^6 \mid (i = 1 \wedge p_i \in \mathcal{D}) \vee$
  $\left(i \in \{2, ..., N-1\} \wedge \|p_i\| \leq \bar{R}_{i-1}\right) \vee$
  $\left(i = i_{cr} \wedge \|p_i\| \leq \bar{R}_{cr}\right)\}$,
  $Dom\left(\zeta_{i1}\right) = \{\tilde{q}_i \in \mathbb{R}^6 \mid (i = 1 \wedge p_i \in \mathcal{D}) \vee$
  $\left(i \in \{2, ..., N-1\} \wedge \|p_i\| \leq \bar{R}_{i-1}\right) \vee$
  $\left(i = i_{cr} \wedge \|p_i\| \leq \bar{R}_{cr}\right)\}$,
  $Dom\left(\zeta_{i2}\right) = \{\tilde{q}_i \in \mathbb{R}^6 \mid (i = 1 \wedge p_i \in \mathcal{D}) \vee$
  $\left(i \in \{2, ..., N-1\} \wedge \|p_i\| > \bar{R}_{i-1}\right) \vee$
  $\left(i = i_{cr} \wedge \|p_i\| > \bar{R}_{cr}\right)\}$,
  $Dom\left(\zeta_{i3}\right) = \{\tilde{q}_i \in \mathbb{R}^6 \mid (i = 1 \wedge p_i \in \mathcal{D}) \vee$
  $\left(i \in \{2, ..., N-1\} \wedge \|p_i\| \leq \bar{R}_{i-1}\right) \vee$
  $\left(i = i_{cr} \wedge \|p_i\| \leq \bar{R}_{cr}\right)\}$,
  $Dom\left(\zeta_{i4}\right) = \{\tilde{q}_i \in \mathbb{R}^6 \mid (i = 1 \wedge p_i \in \mathcal{D}) \vee$
  $\left(i \in \{2, ..., N-1\} \wedge \|p_i\| \leq \bar{R}_{i-1}\right) \vee$
  $\left(i = i_{cr} \wedge \|p_i\| \leq \bar{R}_{cr}\right)\}$ where four of the five discrete states are defined over the set of continuous states for which agent i is inside of its prescribed subdomain $\mathcal{D}^j$. ζ_{i3} (subdomain transfer mode) is defined for agent i outside of its prescribed subdomain,
- A set of edges:
  $E = \{(\zeta_{i0}, \zeta_{i1}), (\zeta_{i1}, \zeta_{i0}), (\zeta_{i1}, \zeta_{i2}), (\zeta_{i0}, \zeta_{i2}), (\zeta_{i2}, \zeta_{i0})$
  $(\zeta_{i1}, \zeta_{i3}), (\zeta_{i3}, \zeta_{i1}), (\zeta_{i3}, \zeta_{i2}), (\zeta_{i3}, \zeta_{i0}), (\zeta_{i3}, \zeta_{i4}),$
  $(\zeta_{i4}, \zeta_{i3}), (\zeta_{i4}, \zeta_{i2})\}$, each of which is a transition that may be triggered by:
- A guard condition:
  $G\left(\zeta_{i0}, \zeta_{i1}\right) = \{\tilde{q}_i \in \mathbb{R}^6 \mid \left(|\hat{e}_i(t)| < \varepsilon_1\right) \wedge$
  $\left((i = 1 \wedge p_i \in \mathcal{D}) \vee \left(i \in \{2, ..., N-1\} \wedge \|p_i\| \leq \bar{R}_{i-1}\right) \vee\right.$
  $\left.\left(i = i_{cr} \wedge \|p_i\| \leq \bar{R}_{cr}\right)\right)\}$ which transitions agent i from local to global coverage when the agent's contribution to the rate of change of the global coverage error drops below some threshold (the coverage rate is insufficient) so long as the agent operates within its prescribed subdomain,
  $G\left(\zeta_{i1}, \zeta_{i0}\right) = \{\tilde{q}_i \in \mathbb{R}^6 \mid \left(\|p_i - p_{\star,i}\| < \varepsilon_2\right) \wedge$
  $\left(\|\Psi_i - \Psi_{\star,i}\| < \varepsilon_3\right) \wedge \left(|\hat{e}_i(t)| \geq \varepsilon_1\right) \wedge$
  $\left((i = 1 \wedge p_i \in \mathcal{D}) \vee \left(i \in \{2, ..., N-1\} \wedge \|p_i\| \leq \bar{R}_{i-1}\right) \vee\right.$
  $\left.\left(i = i_{cr} \wedge \|p_i\| \leq \bar{R}_{cr}\right)\right)\}$ which transitions agent i from global to local coverage when the desired position and orientation has been achieved to within some threshold, the coverage rate is sufficient, and the agent operates within its prescribed subdomain,
  $G\left(\zeta_{i1}, \zeta_{i2}\right) = \{\tilde{q}_i \in \mathbb{R}^6 \mid$
  $\left(i \in \{2, ..., N-1\} \wedge \|p_i\| > \bar{R}_{i-1}\right) \vee$
  $\left(i = i_{cr} \wedge \|p_i\| > \bar{R}_{cr}\right)\}$ which transitions agent i from global coverage to subdomain transfer mode when the agent is not within its prescribed subdomain,
  $G\left(\zeta_{i0}, \zeta_{i2}\right) = \{\tilde{q}_i \in \mathbb{R}^6 \mid$
  $\left(i \in \{2, ..., N-1\} \wedge \|p_i\| > \bar{R}_{i-1}\right) \vee$
  $\left(i = i_{cr} \wedge \|p_i\| > \bar{R}_{cr}\right)\}$ which transitions agent i from local coverage to subdomain transfer mode when the agent is not within its prescribed subdomain,
  $G\left(\zeta_{i2}, \zeta_{i0}\right) = \{\tilde{q}_i \in \mathbb{R}^6 \mid (i = 1 \wedge p_i \in \mathcal{D}) \vee$
  $\left(i \in \{2, ..., N-1\} \wedge \|p_i\| \leq \bar{R}_{i-1}\right) \vee$
  $\left(i = i_{cr} \wedge \|p_i\| \leq \bar{R}_{cr}\right)\}$ which transitions agent i from subdomain transfer mode to local coverage mode when the agent is within its prescribed subdomain,
  $G\left(\zeta_{i1}, \zeta_{i3}\right) = \{\tilde{q}_i \in \mathbb{R}^6 \mid \left(\|p_i - p_{\star,i}\| < \varepsilon_2\right) \wedge$
  $\left(\|\Psi_i - \Psi_{\star,i}\| < \varepsilon_3\right) \wedge \left(|\hat{e}_i(t)| < \varepsilon_1\right) \wedge$
  $\left((i = 1 \wedge p_i \in \mathcal{D}) \vee \left(i \in \{2, ..., N-1\} \wedge \|p_i\| \leq \bar{R}_{i-1}\right) \vee\right.$
  $\left.\left(i = i_{cr} \wedge \|p_i\| \leq \bar{R}_{cr}\right)\right)\}$ which transitions agent i from global coverage to waypoint scan mode (1) when the desired position and orientation has been achieved to within some threshold, the coverage rate is insufficient, and the agent operates within its prescribed subdomain,

$G(\zeta_{i3},\zeta_{i1}) = \{\tilde{q}_i \in \mathbb{R}^6 \mid wp > 13 \wedge$
$\left(|\hat{e}_i(t)| < \varepsilon_1\right) \wedge \left((i = 1 \wedge p_i \in \mathcal{D}) \vee\right.$
$\left(i \in \{2,...,N-1\} \wedge \|p_i\| \leq \bar{R}_{i-1}\right) \vee$
$\left.(i = i_{cr} \wedge \|p_i\| \leq \bar{R}_{cr})\right)\}$ which transitions agent i from waypoint scan mode (1) to global coverage when all 13 subwaypoints have been scanned, the coverage rate is insufficient, and the agent operates within its prescribed subdomain,
$G(\zeta_{i3},\zeta_{i2}) = \{\tilde{q}_i \in \mathbb{R}^6 \mid$
$\left(i \in \{2,...,N-1\} \wedge \|p_i\| > \bar{R}_{i-1}\right) \vee$
$(i = i_{cr} \wedge \|p_i\| > \bar{R}_{cr})\}$ which transitions agent i from waypoint scan mode (1) to subdomain transfer mode when the agent is not within its prescribed subdomain,
$G(\zeta_{i3},\zeta_{i0}) = \{\tilde{q}_i \in \mathbb{R}^6 \mid wp > 13 \wedge$
$\left(|\hat{e}_i(t)| \geq \varepsilon_1\right) \wedge \left((i = 1 \wedge p_i \in \mathcal{D}) \vee\right.$
$\left(i \in \{2,...,N-1\} \wedge \|p_i\| \leq \bar{R}_{i-1}\right) \vee$
$\left.(i = i_{cr} \wedge \|p_i\| \leq \bar{R}_{cr})\right)\}$ which transitions agent i from waypoint scan mode (1) to local coverage when all 13 sub-waypoints have been scanned, the coverage rate is sufficient, and the agent operates within its prescribed subdomain,
$G(\zeta_{i3},\zeta_{i4}) = \{\tilde{q}_i \in \mathbb{R}^6 \mid \|p_i - p_{\star,i}\| < \varepsilon_2 \wedge$
$\left((i = 1 \wedge p_i \in \mathcal{D}) \vee \left(i \in \{2,...,N-1\} \wedge \|p_i\| \leq \bar{R}_{i-1}\right) \vee\right.$
$\left.(i = i_{cr} \wedge \|p_i\| \leq \bar{R}_{cr})\right)\}$ which transitions agent i from waypoint scan mode (1) to waypoint scan mode (2) when the agent has converged upon a sub-waypoint position to within some threshold and the agent operates within its prescribed subdomain,
$G(\zeta_{i4},\zeta_{i3}) = \{\tilde{q}_i \in \mathbb{R}^6 \mid \Psi_i = \Psi_i(t_{G(\zeta_{i3},\zeta_{i4})}) - d\Psi \wedge$
$\left((i = 1 \wedge p_i \in \mathcal{D}) \vee \left(i \in \{2,...,N-1\} \wedge \|p_i\| \leq \bar{R}_{i-1}\right) \vee\right.$
$\left.(i = i_{cr} \wedge \|p_i\| \leq \bar{R}_{cr})\right)\}$ which transitions agent i from waypoint scan mode (2) to waypoint scan mode (1) when the agent has completed a 360° yaw sweep at one of the 13 sub-waypoints and operates within its prescribed subdomain
$G(\zeta_{i4},\zeta_{i2}) = \{\tilde{q}_i \in \mathbb{R}^6 \mid$
$\left(i \in \{2,...,N-1\} \wedge \|p_i\| > \bar{R}_{i-1}\right) \vee$
$(i = i_{cr} \wedge \|p_i\| > \bar{R}_{cr})\}$ which transitions agent i from waypoint scan mode (2) to subdomain transfer mode when the agent is not within its prescribed subdomain,

– A reset map: $R = \{\emptyset\}$ which is empty and included for the sake of completeness.

$\hat{e}_i(t)$, defined in (12), evolves as a function of the time history of the continuous states and essentially represents how well the local coverage protocol is proceeding. ε_1 is a guard value for $\hat{e}_i(t)$, while ε_2 and ε_3 are guard values for position and yaw proximity with respect to the desired values, $p_{\star,i}$ and $\Psi_{\star,i}$, respectively. wp is an index variable for a set of sub-waypoints which defined in Sect. 3.4. $t_{G(\zeta_{i3},\zeta_{i4})}$ is the most recent time at which $G(\zeta_{i3},\zeta_{i4})$ was satisfied. $t_{G(\zeta_{i3},\zeta_{i4})}$ is of relevance because satisfaction of $G(\zeta_{i3},\zeta_{i4})$ requires an agent to yaw around 360° and resume its previous orientation at $t_{G(\zeta_{i3},\zeta_{i4})}$. The variables $\bar{R}_{i-1}$ and $\bar{R}_{cr}$ are the radii of subdomain partitions defined in Sect. 3.1.3 along with i_{cr}. The control laws presented in the vector field definition are derived in the body of the paper.

Note that the case in which $i = 1$ is included as an exit guard condition from ζ_{i2} to ζ_{i0} despite no defined transition for $i = 1$ to ζ_{i2}. This is due to the fact that agent i_{cr} may converge upon $\mathcal{O}$ in the state ζ_{i2} and then become instantaneously reindexed as $i = 1$ upon battery exchange.

6.2 Differentiation under the integral sign

We apply the Reynold's transport theorem (9), a 3-D generalization of the Leibniz integral rule, to (8) in order to compute its time derivative (10). Therefore, it is a necessary condition that both $h\left(C^\star - Q\left(t,\tilde{p}\right)\right)$, i.e. the integrand of (8), and $\frac{\partial}{\partial t}h\left(C^\star - Q\left(t,\tilde{p}\right)\right)$ are continuous over t and $\tilde{p}$.

Lemma 1 $h\left(C^\star - Q\left(t,\tilde{p}\right)\right)$ is continuous in both t and $\tilde{p}$.

Proof It is a well known result that if two functions are continuous in t and $\tilde{p}$, then their difference, product and the maximum of the two functions are all continuous in t and $\tilde{p}$ (Kaczor and Nowak 2003). Note that 0 and $C^\star$ are both constants, and thus continuous in any argument. An assumption of the continuity of $Q\left(t,\tilde{p}\right)$ implies continuity of the difference $C^\star - Q\left(t,\tilde{p}\right)$ which implies continuity of $\max\{0, C^\star - Q\}$. Continuity of products implies that $h\left(C^\star - Q\left(t,\tilde{p}\right)\right) = \max\{0, C^\star - Q\}^3$ is continuous in t and $\tilde{p}$. It remains is to verify that continuity of $Q\left(t,\tilde{p}\right)$ is a valid assumption.

Continuity of $Q\left(t,\tilde{p}\right)$ in t implies that $\forall\epsilon > 0, \exists\delta > 0$ such that $\left|Q\left(t \pm \delta,\tilde{p}\right) - Q\left(t,\tilde{p}\right)\right| < \epsilon$. Note the definition of $Q\left(t,\tilde{p}\right)$ in (6) and (7) and that $S_i\left(\tilde{q}_i(\tau),\tilde{p}\right)$ is upper-bounded by 1 and lower-bounded by 0, regardless of its arguments, $\forall i \in \{1,...,N\}$. The boundedness of the integrand in (6) implies that the existence of an arbitrarily small δ is guaranteed. Continuity in t holds.

$Q\left(t,\tilde{p}\right)$ may be rewritten in terms of its infinite series right-handed Riemann sum:

$$Q\left(t,\tilde{p}\right) = \sum_{i=1}^{N} \lim_{n\to\infty} \sum_{\ell=1}^{n} S_i\left(\tilde{q}_i\left(\ell t n^{-1}\right),\tilde{p}\right)\left(t n^{-1}\right). \quad (58)$$

We may now show continuity of $S_i\left(\tilde{q}_i\left(\ell t n^{-1}\right),\tilde{p}\right), \forall\tilde{p} \in \mathcal{D}$. Note from (3) and (5) that $S_i\left(\tilde{q}_i\left(\ell t n^{-1}\right),\tilde{p}\right)$ is defined over all of $\mathcal{D}$ but takes nonzero values only within $\mathcal{S}_i$, as parametrized by continuous constraint functions $C_{ki}, \forall k \in \{1,2,3\}$, and is defined as zero along the boundary $\partial\mathcal{S}_i$. As $S_i\left(\tilde{q}_i\left(\ell t n^{-1}\right),\tilde{p}\right) \to 0$ as $\tilde{p} \to \partial\mathcal{S}_i$

from any direction in $\mathbb{R}^3$, we have that $S_i\left(\tilde{q}_i\left(\ell t n^{-1}\right),\tilde{p}\right)$ is continuous $\forall \tilde{p} \in \mathcal{D}$. This continuity holds through summation in (58) as well. This concludes the proof.

Lemma 2 $\frac{\partial}{\partial t} h\left(C^{\star} - Q\left(t,\tilde{p}\right)\right)$ is continuous in both t and $\tilde{p}$.

Proof In *Lemma 1* it is shown that $Q\left(t,\tilde{p}\right)$ and thus $\max\{0, C^{\star} - Q\left(t,\tilde{p}\right)\}^3$ are continuous in t and $\tilde{p}$. Taking the time derivative we have that $\frac{\partial}{\partial t} h\left(C^{\star} - Q\left(t,\tilde{p}\right)\right) = \left(-3\max\{0, C^{\star} - Q\left(t,\tilde{p}\right)\}^2\right)\left(\frac{\partial Q}{\partial t}\right)$ is continuous in the first multiplicative term. It remains to show that $\frac{\partial Q}{\partial t}$ is continuous in t and $\tilde{p}$. Recall from (6) and (7) that:

$$Q\left(t,\tilde{p}\right) = \sum_{i=1}^{N} \int_0^t S_i\left(\tilde{q}_i\left(\tau\right),\tilde{p}\right) d\tau. \tag{59}$$

It is shown in *Lemma 1* that $S_i\left(\tilde{q}_i\left(\tau\right),\tilde{p}\right)$ is continuous in $\tilde{p}$. Continuity in t is guaranteed as the state of $\mathcal{S}_i$ is determined by the position and orientation of agent i for which discontinuity is physically impossible. Thus (59) meets all necessary conditions for differentiation via the first fundamental theorem of calculus:

$$\frac{\partial Q\left(t,\tilde{p}\right)}{\partial t} = \sum_{i=1}^{N} \frac{\partial}{\partial t} \int_0^t S_i\left(\tilde{q}_i\left(\tau\right),\tilde{p}\right) d\tau = \sum_{i=1}^{N} S_i\left(\tilde{q}_i\left(\tau\right),\tilde{p}\right).$$

which is continuous in t and $\tilde{p}$ as verified above and in *Lemma 1*. This concludes the proof.

6.3 A supporting lemma

Lemma 3 Under the assumption that $x \leq y$ and that $x \geq 2$, one may conclude that:

$$\frac{x^3}{x-1} \leq \frac{y^3}{y-1}.$$

Proof The assumptions directly provide the following:

$2 \leq x \leq y.$

Subtract 1:

$1 \leq x - 1 \leq y - 1,$

invert all terms, and then rearrange into the equivalent statement:

$$\frac{1}{y-1} \leq \frac{1}{x-1} \leq 1.$$

We may refer to $\{\frac{1}{y-1}, \frac{1}{x-1}\}$ and $\{\frac{1}{x-1}, 1\}$ as similarly ordered sets. Chebyshev's Sum Inequality Theorem as presented in Hardy et al (1952) may be applied to these similarly ordered sets to yield:

$$\frac{1}{(y-1)(x-1)} + \frac{1}{x-1} \geq \frac{1}{2}\left(\frac{1}{y-1} + \frac{1}{x-1}\right)\left(\frac{1}{x-1} + 1\right).$$

Now simplify and rearrange as follows:

$$\frac{1}{(y-1)(x-1)} + \frac{1}{x-1} \geq \frac{1}{2}\left(\frac{1}{y-1} + \frac{1}{x-1}\right)\left(\frac{x}{x-1}\right),$$

$$\frac{1}{(y-1)(x-1)} + \frac{1}{x-1} \geq \frac{1}{2}\left(\frac{x}{(y-1)(x-1)} + \frac{x}{(x-1)^2}\right),$$

$$\frac{1}{(y-1)(x-1)} + \frac{1}{x-1} \geq \frac{\frac{1}{2}x}{(y-1)(x-1)} + \frac{\frac{1}{2}x}{(x-1)^2},$$

$$\frac{1}{x-1} \geq \frac{\frac{1}{2}x - 1}{(y-1)(x-1)} + \frac{\frac{1}{2}x}{(x-1)^2}.$$

Multiply by $2x^2(x-1)$:

$$2x^2 \geq \frac{x^3 - 2x^2}{y-1} + \frac{x^3}{x-1},$$

and rearrange to form:

$$\frac{x^3}{x-1} \leq 2x^2 - \frac{x^3 - 2x^2}{y-1}. \tag{60}$$

Thus, the proof will be completed by verifying that the right hand side of (60) is less than or equal to $\frac{y^3}{y-1}$ under the assumptions provided by the lemma. Noting the fact that:

$$2x^2 - \frac{x^3 - 2x^2}{y-1} = \frac{2x^2 y - x^3}{y-1},$$

this is equivalent to verifying that $2x^2y - x^3 \leq y^3$ for $y \geq x$. This is straight forward:

$(x-y)^2 \geq 0,$

$x^2 + y^2 - 2xy \geq 0,$

$x^3 + xy^2 - 2x^2y \geq 0,$

and thus for $y \geq x$:

$2x^2y \leq x^3 + xy^2 \leq x^3 + y^3.$

This verifies the condition $2x^2y - x^3 \leq y^3$. Therefore, (60) may be rewritten as:

$$\frac{x^3}{x-1} \leq 2x^2 - \frac{x^3 - 2x^2}{y-1} \leq \frac{y^3}{y-1},$$

$$\frac{x^3}{x-1} \leq \frac{y^3}{y-1}.$$

This concludes the proof.

References

Abazeed M, Faisal N, Zubair S, Ali A (2013) Routing protocols for wireless multimedia sensor network: A survey. Journal of Sensors 2013

Arajo JF, Sujit PB, Sousa JB (2013) Multiple UAV area decomposition and coverage. In: 2013 IEEE Symposium on Computational Intelligence for Security and Defense Applications (CISDA), pp 30–37

Atinc G, Stipanovíc DM, Voulgaris PG (2014) Supervised coverage control of multi-agent systems. Automatica 50(11):2936–2942

Beard RW (2008) Quadrotor dynamics and control, lecture notes

Bentz W, Panagou D (2016) An energy-aware redistribution method for multi-agent dynamic coverage networks. In: Proc. of the 2016 IEEE Conference on Decision and Control, Las Vegas, NV

Bentz W, Panagou D (2017) 3D dynamic coverage and avoidance control in power-constrained UAV surveillance networks. In: Proc. of the 2017 International Conference on Unmanned Aircraft Systems, Miami, FL

Berman E, Fladeland M, Liem J, Kolyer R, Gupta M (2012) Greenhouse gas analyzer for measurements of carbon dioxide, methane, and water vapor aboard an unmanned aerial vehicle. Sensors and Actuators B: Chemical 169:128–135

Chahine MT, Chen L, Dimotakis P, Jiang X, Li Q, Olsen ET, Pagano T, Randerson J, Yung YL (2008) Satellite remote sounding of mid-tropospheric CO2. Geophysical Research Letters 35(17)

Cheng P, Keller J, Kumar V (2008) Time-optimal UAV trajectory planning for 3D urban structure coverage. In: Proc. of the 2008 IEEE/RSJ International Conference on Intelligent Robots and Systems, Nice, France, pp 2750–2757

Cole DT, Goktogan AH, Thompson P, Sukkarieh S (2009) Mapping and tracking. IEEE Robotics Automation Magazine 16(2):22–34

Cortes J, Martínez S, Karatas T, Bullo F (2004) Coverage control for mobile sensing networks. IEEE Trans on Robotics and Automation 20(2):243–255

Franco C, Stipanovi DM, Lpez-Nicols G, Sags C, Llorente S (2015) Persistent coverage control for a team of agents with collision avoidance. European Journal of Control 22:30–45

Hardy GH, Littlewood JE, Pólya G (1952) Inequalities. Cambridge UP, pg. 43

Hokayem P, Stipanovíc D, Spong M (2007) On persistent coverage control. In: Proc. of the 2007 IEEE Conference on Decision and Control, New Orleans, LA, USA, pp 6130–6135

Hübel N, Hirche S, Gusrialdi A, Hatanaka T, Fujita M, Sawodny O (2008) Coverage control with information decay in dynamic environments. In: Proc. of the 17th IFAC World Congress, Seoul, South Korea, pp 4180–4185

Hussein II, Stipanović DM (2007) Effective coverage control for mobile sensor networks with guaranteed collision avoidance. IEEE Trans on Control Systems Technology 15(4):642–657

Kaczor W, Nowak M (2003) Problems in mathematical analysis II. American Mathematical Society

Kwok A, Martínez S (2008) Deployment algorithms for a power-constrained mobile sensor network. In: Proc. of the 2008 IEEE International Conference on Robotics and Automation, Pasadena, CA, pp 140–145

Leahy K, Zhou D, Vasile CI, Oikonomopoulos K, Schwager M, Belta C (2016) Persistent surveillance for unmanned aerial vehicles subject to charging and temporal logic constraints. Autonomous Robots 40(8):1363–1378

Liang J, Liu M, Kui X (2014) A survey of coverage problems in wireless sensor networks. Sensors and Transducers pp 240–246

Liu B, Dousse O, Nain P, Towsley D (2013) Dynamic coverage of mobile sensor networks. IEEE Transactions on Parallel and Distributed systems 24(2):301–311

Lygeros J (2004) Lecture notes on hybrid systems, eNSIETA course

Ma X, Jiao Z, Wang Z, Panagou D (2016) 3D Decentralized Prioritized Motion Planning and Coordination for High-Density Operations of Micro Aerial Vehicles. accepted for publication in the IEEE Transactions on Control Systems Technology, to appear. `http://www-personal.umich.edu/~dpanagou/assets/documents/XMa_TCST17.pdf`

Mitchell D, Corah M, Chakraborty N, Sycara K, Michael N (2015) Multi-robot Long-Term Persistent Coverage with Fuel Constrained Robots. In: Proc. of the 2015 IEEE International Conference on Robotics and Automation (ICRA), pp 1093–1099

Nam LH, Huang L, Li XJ, Xu JF (2016) An approach for coverage path planning for uavs. In: 2016 IEEE 14th International Workshop on Advanced Motion Control (AMC), pp 411–416

Oktug S, Khalilov A, Tezcan H (2008) 3D coverage analysis under heterogeneous deployment strategies in wireless sensor networks. In: Proc. of the 2008 Fourth Advanced International Conference on Telecommunications, pp 199–204

Panagou D, Stipanović DM, Voulgaris PG (2016) Distributed coordination control for multi-robot networks using Lyapunov-like barrier functions. IEEE Trans on Automatic Control 61(3):617–632

Panagou D, Stipanović DM, Voulgaris PG (2016, in press) Distributed dynamic coverage and avoidance control under anisotropic sensing. accepted as Full Paper in IEEE Transactions on Control of Network Systems, to appear (available online)

Piciarelli C, Micheloni C, Foresti GL (2011) Automatic reconfiguration of video sensor networks for optimal 3d coverage. In: Proc. of the 2011 Fifth ACM/IEEE International Conference on Distributed Smart Cameras (ICDSC), IEEE, pp 1–6

Rinaldi F, Chiesa S, Quagliotti F (2013) Linear quadratic control for quadrotors uavs dynamics and formation flight. Journal of Intelligent & Robotic Systems 70(1):203–220

Slattery JC (1999) Advanced Transport Phenomena. Cambridge UP

Smith SL, Schwager M, Rus D (2012) Persistent robotic tasks: Monitoring and sweeping in changing environments. IEEE Transactions on Robotics 28(2):410–426

Song C, Liu L, Feng G, Wang Y, Gao Q (2013) Persistent awareness coverage control for mobile sensor networks. Automatica 49(6):1867–1873

Stipanović DM, Valicka C, Tomlin CJ, Bewley TR (2013) Safe and reliable coverage control. Numerical Algebra, Control and Optimization 3:31–48

Tisdale J, Kim Z, Hedrick JK (2009) Autonomous uav path planning and estimation. IEEE Robotics Automation Magazine 16(2):35–42

Wills AG, Heath WP (2002) A recentred barrier for constrained receding horizon control. In: Proc. of the 2002

American Control Conference (IEEE Cat. No.CH37301), vol 5, pp 4177–4182 vol.5

Xie L, Zhang X (2013) 3D clustering-based camera wireless sensor networks for maximizing lifespan with minimum coverage rate constraint. In: Proc. of the 2013 IEEE Global Communications Conference (GLOBECOM), IEEE, pp 298–303

Yang M, Kim D, Li D, Chen W, Du H, Tokuta AO (2013) Sweep-Coverage with Energy-Restricted Mobile Wireless Sensor Nodes, Springer Berlin Heidelberg, Berlin, Heidelberg, pp 486–497

Zhang Y, Li X, Yang J, Liu Y, Xiong N, Vasilakos AV (2013) A real-time dynamic key management for hierarchical wireless multimedia sensor network. Multimedia Tools and Applications 67(1):97–117

Zhu C, Zheng C, Shu L, Han G (2012) A survey on coverage and connectivity issues in wireless sensor networks. Journal of Network and Computer Applications 35(2):619–632